TESLA Report 2005-08
Hamburg 28.02.2005

First Generation of Optical Fiber Phase Reference Distribution System for TESLA

Krzysztof Czuba[a], Frank Eints[b], Matthias Felber[b],
Janusz Dobrowolski[a], Stefan Simrock[b],

[a] Institute of Electronic Systems, Warsaw University of Technology, ELHEP Group, ZUiAM, Nowowiejska 15/19, 00-665 Warsaw, Poland

[b] Deutsches Elektronen-Synchrotron DESY

1. ABSTRACT

This report describes the design of a phase stable Fiber Optic (FO) link for the TESLA technology based projects. The concept of this long optical link, with a feedback system suppressing long term drifts of the RF signal phase is described. Stability requirements are given and most important design issues affecting the system performance are discussed. The technical design issues of system components like laser transmitter and optical phase shifter are described in detail. Last sections depict the software developed for system control and experimental results obtained after system was assembled.

INDEX

2. INTRODUCTION

The UV Free-Electron Laser (UVFEL) and the TeV-Energy Superconducting Linear Accelerator (TESLA) [1] projects will require phase synchronization of 0.1ps short term (millisecond), 1ps short term (minutes) and 10ps long term (days). The stringent synchronization requirement of 10fs (short term) was given for the X-Ray Free-Electron Laser (XFEL) [2]. To fulfill this requirement the XFEL may use a fiber laser as reference generator. But this requirement applies for a special location only, therefore the RF phase reference distribution system developed for UVFEL and TESLA may successfully be used in the XFEL.

The fiber optic system described in this document will be a part of the phase reference distribution system which is prepared for the TESLA technology based projects [3]. The phase reference distribution system will consist of a Master Oscillator (MO), long phase stable Fiber-Optic (FO) links (subject of this document) and short (< 500 m) coaxial cable based distribution sections. The system will be providing a phase stable signal to multiple RF devices located along the accelerator.

The work on the project was performed in DESY Hamburg in cooperation with Institute of Electronic Systems from Warsaw University of Technology. The work on the project started in the second quarter of the year 2003 and the project state described in this document was finished in October 2004.

Different types of phase errors and different stability types can be distinguished. The shortest stability type (measured over e.g. milliseconds time) corresponds mainly to phase noise performance of the system components. Devices that mostly dictate the phase noise level in the system are the MO and frequency multipliers. The optical link also influences the phase noise and the laser transmitter should be considered as the main noise source. The phase noise performance of the link can be improved by connecting a low noise phase-locked Voltage Controlled Oscillator (VCO) at the link output.

The short (measured over minutes) and long (days) term stability of the system is mainly influenced by environmental effects like temperature or other physical parameters changes and also by effects due to aging of the system components. Temperature is the most important source of phase drifts in the long link. Typical phase length vs. temperature coefficient of a fiber-optic cable K = ~10 ppm/^{o}C. The primary contribution to the temperature coefficient in fiber is the change in the refractive index. As it will be calculated and measured in this document, a temperature change of few ^{o}C on kilometers long link would cause a signal phase error of several hundred degrees. This error is much more than the maximum allowable phase error and it must be suppressed with a factor of hundreds using feedback on phase. The system described in this document offers the possibility of suppressing temperature induced long term signal phase drifts and it was successfully tested in laboratory conditions.

Very good long term output signal phase stability has been obtained. Therefore the FO system can be used for long term phase monitoring purposes at specified locations in the distribution system. The FO link can also be used as a distribution line for longer distances but after a phase stable VCO used for phase noise performance improvement - as it was mentioned above.

3. SYSTEM REQUIREMENTS AND CONCEPT

Requirements on the system concern mostly signal phase stability at the end of the distribution line. The definition of stability types is given in chapter 2. Design requirements on the system performance are listed below:

- Short term stability (phase noise) << 1ps , 10fs at one location in the XFEL
- Short term stability (minutes) < 1ps at RF frequency (0.5^o @1.3 GHz)
- Long term stability (days) < 10ps within days (5.0^o @1.3 GHz)
- System length up to 15km
- Distributed frequencies 9 - 2856MHz
- High reliability
- Easy installation and maintenance (modular design)
- As low as possible system cost, because many copies of the system will be built and installed.

The system concept has been developed for the NLC project [4]. Figure 3.1 shows the block diagram of the system suited to the TESLA project needs. The RF signal from the reference generator modulates the light amplitude in a 1550 nm DFB laser which sends the light into the fiber-optic cable. An adjustable fiber-optic phase shifter is connected in series with the main fiber (long link). Signal travels through the entire link up to the mirror terminating end of the link. Then, reflected, it travels back the same way up to the optical circulator and further to the optical receiver A (called further FO RxA). The difference between the phase of the stable input signal and the signal that traveled twice throughout the entire long link is measured by the phase detector. Assuming that the transmitted and reflected optical signals propagate at the same speed (system symmetry), one can obtain error voltage carrying precise information of the phase change in the long link fiber. The phase change observed at FO RxA is twice the change observed at FO RxB. The error voltage is used to adjust the phase length in the phase shifter to decrease the phase error by means of a feedback loop. The phase at the very end of the link is stabilized by holding the constant level of the detector output voltage. In other words, the reflected signal phase is kept stable. By this any symmetrical phase error that appears in the long link can be suppressed – more detailed considerations on errors are given in section 4.

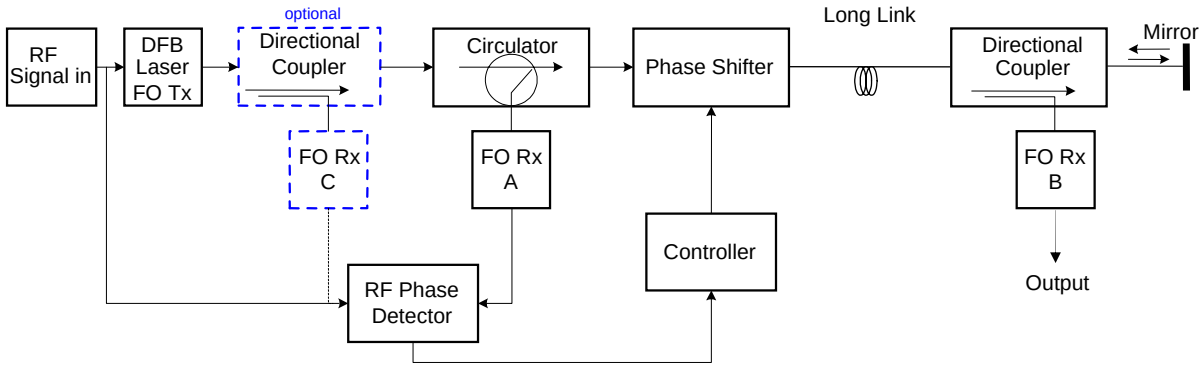

Figure 3.1: *System block diagram*

It must be noticed that the phase of the signal traveling through the long link fiber is controlled only at the mirror. Significant, local temperature variations may occur along the

accelerator in normal operating conditions. Therefore it is not recommended to make pick up points far from the mirror. This scheme can be used for point-to-point link application only.

Optional directional coupler and F.O. receiver C shown in Fig. 3.1 can be used for monitoring of phase drifts in the laser transmitter and correcting for errors in the long link. Of course additional phase detector and controller input would be necessary. If the laser is temperature controlled, there is no need to use these optional components.

4. CONSIDERATIONS ON SOURCES OF ERRORS

Several sources of phase errors were considered in the FO system. In the previous chapter required error values are given in the units of ps and degree. Unit conversion can be performed by calculating the time of one RF signal period which corresponds to 360^o of phase change. Comparing given error in degrees to 360^o and the time of signal period, error in ps unit can be calculated.

4.1. TEMPERATURE

Temperature is the most important source of phase drifts in the system, therefore more attention is put to this problem and a method for quantifying temperature induced errors is given.

Typical fiber-optic cable has a phase length vs. temperature coefficient of K = ~10 ppm/^{o}C. The primary contribution to the temperature coefficient in fiber is the change in the refractive index. The phase change of the signal at the end of a fiber-optic cable, at given RF frequency and for given temperature change (e.g. per 1^{o}C), can be calculated proceeding the following way: Assume a link of length L made of fiber with effective refractive index N_{eff}. The light velocity in the fiber can be found by simple equation 4.1.1 where c_0 is the light velocity in vacuum.

$$c = \frac{c_0}{N_{eff}} \quad [\text{m/s}] \tag{4.1.1}$$

The time required by light to travel through the entire link length L is described by equation:

$$t = \frac{L}{c} \qquad [\text{s}]$$

Knowing the fiber temperature change ΔT, and the temperature coefficient K the light travel time change Δt can be found from equation:

$$\Delta t = tK\Delta T \qquad [\text{s}]$$

One RF signal period time equal $1/f_{RF}$ (RF signal frequency) corresponds to $\varphi = 360^o$ of signal phase. Comparing this time to Δt the equation 4.1.2 can easily be derived, which describes the RF signal phase change in the link length L, after temperature change of ΔT:

$$\Delta\varphi = 360^o\, f_{RF}\Delta t \quad [^o] \tag{4.1.2}$$

In the case of the FO link (f_{RF} = 1.3 GHz, SMF-28 fiber type) $\Delta\varphi$ equals ~22.9^o per 1 km and 1^{o}C. For long time (e.g. from summer to winter) a 10^{o}C of temperature change can be assumed. If the MO will be placed in the middle of the accelerator, then the longest

distribution link will be half of the accelerator length – assume 15 km. Then the total phase change of 1.3 GHz RF signal will be **3435^o ! –** the required limit on the long term stability is exceeded more than 650 times, meaning that signal distribution is impossible without a compensation of the temperature drifts.

The fiber temperature could be stabilized, but it would require the temperature stability of ~0.001^{o}C. Fulfilling such requirement may be very difficult or impossible, but for sure very expensive, taking into account the system dimension. Fortunately, the phase of the signal is affected by temperature symmetrically when the signal is traveling in both directions through the system. So **phase drift caused by temperature change on the long link is a symmetrical error and can be compensated by the feedback system** (as described in chapter 3).

The phase error in the long link (e.g. 15 km length and 10^{o}C temperature change) can be suppressed by using a spool with shorter fiber (e.g. 5 km) connected in series with the long link fiber and regulating spool temperature in temperature controlled oven in opposite direction than main fiber temperature (for given example -30^{o}C). The spool with fiber inside the temperature controlled oven will be used as an optical phase shifter (see figure 3.1).

4.2. CHANGES OF THE INPUT FREQUENCY

Reference oscillator frequency drifts (unavoidable even in high quality devices) may be a reason for significant phase changes at the end of the long link of any type. Below considerations are given for quantifying this type of error in optical fiber but same method can be used for quantifying errors in the coaxial cable or waveguide.

Assume link length L, signal frequency f and signal velocity in the optical fiber given by the equation 4.1.1. Number of RF signal wavelengths in the link (assumed is light amplitude modulation by sine wave):

$$N = \frac{L}{\lambda} = \frac{Lf}{c}$$

If the signal frequency change is $\Delta f = f_1 - f$, then the number of wavelengths changes as

$$\Delta N = N - N_1 = L\frac{f_1}{c} - L\frac{f}{c} = \frac{L}{c}\left(f_1 - f\right) = \frac{L}{c}\Delta f$$

The phase change at the output of the long link (measured by phase detector) is

$$\Delta\varphi = 360^o\,\Delta N \ ^{1}$$

This type of phase error must be clearly distinguished from phase error between two signals with different frequency. As it is commonly known, phase difference between sine type signals with different frequency, changes as a linear function of time and can change up to infinity. Considerations given in this section concern phase difference on the signal provided from one source measured between the beginning and the end of a long distribution line.

Calculation example:

[1] Assuming that the phase change at the second input of the phase detector is 0^o

Light velocity in the SMF28 fiber: $c = \frac{3*10^8}{1.468} = 2.043*10^8[\frac{m}{s}]$

Assume f = 1.3 GHz. Wavelength of the signal in fiber: $\lambda_{1.3} = 0.157$ [m]

The frequency stability factor of quartz crystal oscillator is obtained in the range of 10^{-7}. Multiplied by f it gives 130 Hz of possible frequency change. For simplicity assume f_1 = 1.3 GHz +100 Hz and system length L=10 km.

$$\Delta\varphi = 360^o \frac{10000m}{2.043*10^8 \frac{m}{s}} 100\frac{1}{s} = 1.76^o$$

It corresponds to 3.52 ps of error in the time domain. If such frequency drift appears within minute time, it already causes that phase stability (1 ps) requirement given in chapter 3 is not fulfilled.

Influence of input signal frequency changes on the FO system performance

In the system there are two signal outputs: called A – for the feedback controller and B – long link output. See figure 4.2.1. Rx – means here the optical receiver.

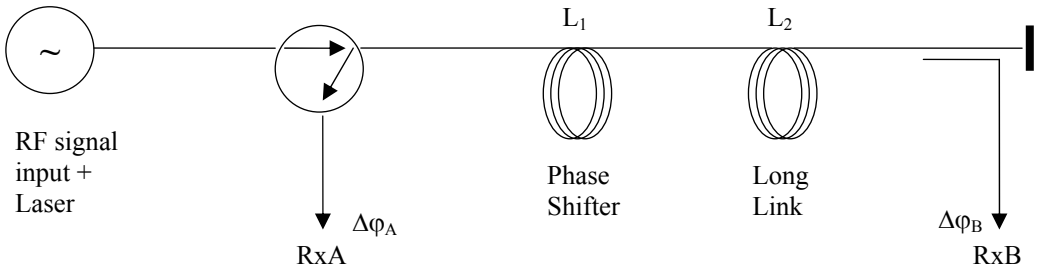

Figure 4.2.1: *Simplified FO system diagram for error consideration*

To the receiver B, signal travels only once through the phase shifter (with fiber length L_1) and long link (fiber length L_2), so phase change due to input frequency change of Δf equals:

$$\Delta\varphi_B = 360^o \frac{L_1 + L_2}{c}\Delta f \qquad (4.2.1)$$

To the receiver A, signal travels twice through the phase shifter and the long link, therefore phase change due to input frequency change of Δf is equal:

$$\Delta\varphi_A = 360^o \frac{2(L_1 + L_2)}{c}\Delta f = 2\Delta\varphi_B \qquad (4.2.2)$$

Equation 4.2.1 gives the value of the phase error "observed" by the system controller. The phase in the long link will be compensated by the feedback loop for $-\Delta\varphi_A$. It will be compensated for both directions, so at the end of the link phase change will be $-0.5\Delta\varphi_A = -\Delta\varphi_B$. It means that error will be cancelled for the RxB output. Of course, if the frequency is drifting slower than system response and the signal path from the circulator to the RxA is small in comparison with L_1+L_2.

The result is that slow frequency drifts cause no errors in the system!

4.3. FIBER OPTIC TRANSMITTER AND RECEIVER

The transmitter (FO Tx) and both optical receivers (FO Rx) may also be a significant source of phase errors. Let us focus on the FO Tx and RxA first. Errors added by these components can not be removed by the feedback because FO Tx and FO RxA are located asymmetrically in the system. Assume that the only source of phase error is FO Tx. A simplified diagram of the system is presented in figure 4.3.1.

If a phase error $\Delta\varphi_{Tx}$ appears in the transmitter, it is transported to the output of the link, so $\Delta\varphi_{out} = \Delta\varphi_{Tx}$. The same error is also transmitted back to the phase detector input $\Delta\varphi_A=\Delta\varphi_{Tx}$. To correct this error (make $\Delta\varphi_A = 0$), the phase length is adjusted in the phase shifter. But since the phase of the optical signal traveling to the end of the link and back is affected twice by the phase shifter activity, after correcting for $-\Delta\varphi_A$ at the FO RxA input, the phase length adjustment equals $-0.5\Delta\varphi_A$ in one signal travel direction. Therefore the phase of the output signal will be corrected for $-0.5\Delta\varphi_A$ and the output phase error will be $\Delta\varphi_{out\_corrected} = \Delta\varphi_{Tx} - 0.5\Delta\varphi_A = 0.5\Delta\varphi_A$.

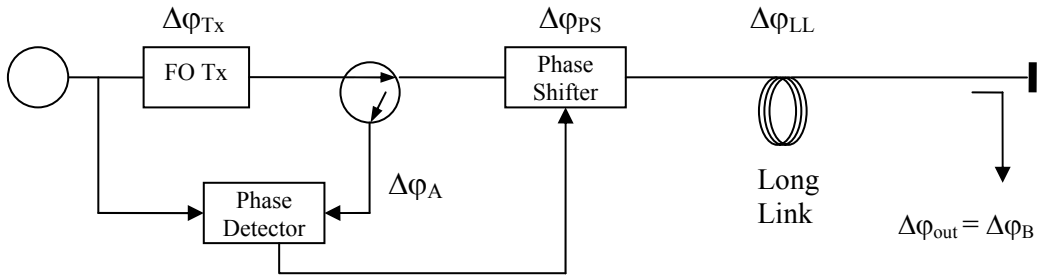

Figure 4.3.1: *Simplified system diagram for transmitter error influence on the FO system performance.*

The same output signal phase error value will occur when an error ($\Delta\varphi_A$) appears in the FO RxA – because RxA is also located asymmetrically in the system. But this error does not appear directly at the output of the system because the FO RxA is located outside of the main signal path ($\Delta\varphi_{out}$=0 before loop activity). Feedback loop "sees" the FO RxA error (equal $\Delta\varphi_A$) at the output of the phase detector and corrects for $-\Delta\varphi_A$. The output error will be $\Delta\varphi_{out} = -0.5\Delta\varphi_A$ (with negative sign). This is an important observation because it means that **phase error appearing in the laser and the receiver A is suppressed with the factor of two**. Of course only slow phase drifts – within the bandwidth of the feedback loop can be suppressed.

If the phase error appears in the receiver B, then it can not be suppressed because the FO RxB is located outside of the feedback loop. Measured was the FO Tx and FO Rx performance by changing its temperature in the range of 10^oC and measuring signal phase change. Detected signal phase change at the FO Tx output was $<0.1^o/^oC$, and at the FO Rx output it was $<0.05^o/^oC$ (chapter 8). These errors must be considered and an option of keeping sensitive components temperature stable by putting them into a temperature controlled chamber is planned.

4.4. CIRCULATOR CROSS TALK IN THE FO SYSTEM

The cross talk between the input port and the return port of the optical circulators is finite. Therefore there will always be a small optical signal (A in figure 4.4.1) interfering with the signal B that traveled through the entire system and back to the circulator. In a very long link

the optical loss can be so high that power level of signals A and B may be comparable. Let's find the influence of the interference on the measurement result.

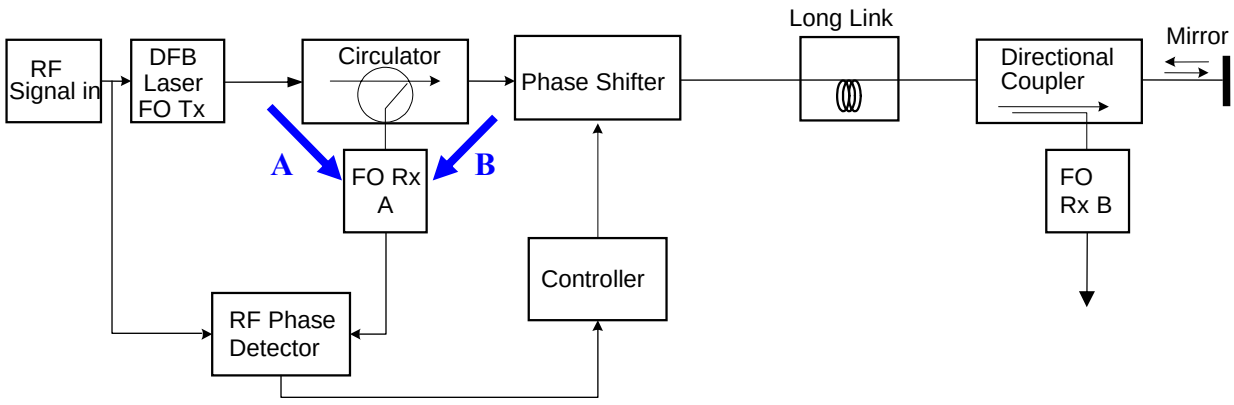

Figure 4.4.1: *Phase error due to finite circulator cross talk*

The amplitude and phase of both signals (depicted A and B in figure 4.4.1) can be specified relatively to the master oscillator signal parameters. Signals A and B interfere at the FO receiver (FO Rx A) input and their sum is signal C – see fig. 4.4.2 – that is measured by the phase detector. If the phase difference between signals A and B is equal 0 or 180^o then the measured phase error will be 0. In the worst case – when the phase difference between A and B is equal 90^o or 270^o – the measured phase error α will be maximum.

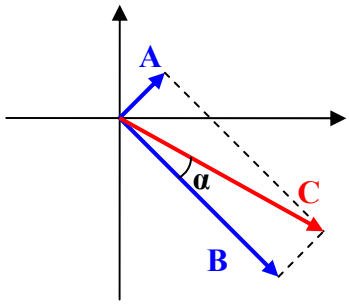

Figure 4.4.2: *Interfering signals at the FO RxA inptut.*

The maximum phase error can be calculated using following procedure:

$$\alpha = \arctan(\frac{A}{B}) \qquad (4.4.1)$$

Assume that the amplitude of A is a fraction of the amplitude of B, $\frac{A}{B} = \Delta U$. The power level difference ΔP between signals A and B can be found when the circulator cross talk value and the loss of the fiber-optic link is known. Optical loss is usually given in power dB units. Since the signal power level changes with the power of 2 related to the voltage level, the power difference ΔP_{dB} (in dB units) corresponds to ΔP and $\Delta U = \Delta P^{1/2}$ in a linear scale. Therefore the amplitude difference can be found from following equation:

$$\Delta U = 10^{\frac{\Delta P_{dB}}{20}} \qquad (4.4.2)$$

Inserting equation 4.4.2 into 4.4.1 the equation for the maximum phase error (4.4.3) is obtained:

$$\alpha = \arctan\left(\left|10^{\frac{\Delta P}{20}}\right|\right) \qquad (4.4.3)$$

Table 4.4.1: Example error values:

ΔP [dB]	A [°]
-5	29.350
-10	17.548
-15	10.083
-20	5.710
-25	3.218
-30	1.811
-35	1.018
-40	0.572
-45	0.322
-50	0.181
-55	0.101

CONCLUSION:

Circulator cross talk is a very important source of errors because in the long link (15 km) the attenuation of the optical signal (after including losses in optical components) may be so large than signal power difference will reach value of -15 to -25 dB. Assuming that standard circulator with 40 dB cross talk is used.

Fortunately, during system operation, the phase of the output signal is stabilized by maintaining constant the phase difference between the signal from the RF source and the signal from the FO RxA. Therefore even if described error appears, it will be constant in time and can be considered as zero because only variable phase errors are the matter of concern in the phase reference distribution system.

5. SUBSYSTEM PARAMETERS

Summary of issues and parameter lists concerning the components used in the FO system is given in this chapter.

5.1. FIBER

Standard, low cost SMF-28 fiber manufactured by Corning company
Single mode fiber optic chosen for better signal performance
1550nm wavelength to minimize optical loss
Loss: < 0.22dB/km @ λ=1550nm => 5km fiber: 1.1dB; 20km fiber: 4.4dB

5.2. LASER TRANSMITTER

AGERE 2502G, DFB type laser module, optical wavelength 1550nm
Desired 3dB bandwidth 2.856 GHz (maximum frequency available in the Master Oscillator – may not be necessary to distribute via optical fiber), required 1.3 GHz

Slope efficiency 0.1 mW/mA (typ.) (-20 dB^2W/A)
Design of laser transmitter (FO Tx) module is described in detail in section 6.3.

5.3. FIBER-OPTIC RECEIVER

Fiber optic receiver manufactured by Spinner.
Typical photodiode module integrated with fiber-optic connector.
Optical wavelength 1550nm (1200...1600nm)
Optical input power: -15dBm…+3dBm
Minimum bandwidth 2.856GHz
Gain: +20dB
Optical reflection: <-55dB
1dB compression point: 17,5dBm
Output resistance: 50Ω

5.4. DIRECTIONAL COUPLER, CIRCULATOR

Fiber optic, pigtailed devices
Circulator (OC-3-λ, manufactured by OFR): power = 2-5W cw
loss = 0.73dB (Port 1 to 2), 0.8dB (Port 2 to 3)
isolation = >35dB (3 to 2 and 2 to 1), >40dB (1 to 3)
Directional coupler, manufactured by Huber+Suhner:
loss: main line: 0.21dB
coupled line: 20.5dB

5.5. FIBER-OPTIC CONNECTORS

FC/APC type chosen for minimum reflections
Loss = 0.2dB per connection
Back reflections < -60dB

5.6. PHASE SHIFTER

The range of RF signal phase change (~3500^o) that must be compensated with a phase shifter was calculated in the section 4.1. This value corresponds to the range of $2*10^6 * 2\pi$ of 1550 nm light phase change.

Commercial optical phase shifters with typical 20π light phase change can be found. Motorized optical delay lines operate up to 20 cm of optical length change, which corresponds to roughly 350^o phase change of the RF 1.3 GHz signal. Such a range is 10 times less than required. It should be mentioned here that prices of commercial phase shifters start from 1000$ per device.

The best solution seems to be optical fiber on a spool inside of the temperature controlled oven (as mentioned in section 4.1). A spool with 5 km of fiber inside an oven with 30^oC temperature range can be used to compensate for signal phase changes induced by 10^oC temperature changes of the link with 15 km length. Special temperature controlled oven (**called further oven 1**) was developed for this purpose. The design of oven 1 is described in section 6.1.

5.7. MIRROR

Fiber optic reflector with Gold Tipped 1m long 1550nm fiber
FC/APC optical connectors
Mirror efficiency: 85% => loss = 0.7dB

5.8. PHASE DETECTOR

Commercial phase detector integrated circuit (HMC 403) manufactured by the Hittite company was used. A printed circuit board was designed for this chip.
Operating frequency range reaches 1.3GHz.
For higher frequencies down-converter would be required (future plan, not relevant in this document).

5.9. FEEDBACK CONTROLLER

PID controller is suitable (more details in the section 7.2). Digital implementation of the controller was chosen for higher flexibility of device development. Because of very slow temperature changes, the bandwidth of the controller could be very low and the sampling frequency of the analogue to digital (ADC) and digital to analogue (DAC) converters could be as low as 1 Hz.

For the laboratory system development a MSC1211 microcontroller board (by Texas Instruments) with ADC and DAC was used. The microcontroller board was connected to the PC with Matlab software installed. A Graphical User Interface (GUI) was developed to simplify system development and measured data observation (described in detail in chapter 7).

In the future the system controller will be embedded in PC independent card.

5.10. TUNNEL CONDITION SIMULATOR – OVEN 2

Another temperature controlled oven (**called further oven 2**) was required to simulate temperature changes in the tunnel for system performance tests. A spool with 20 km of fiber inside the oven 2 was used in the system as a long link (see figure 3.1). Oven temperature was changed and system response and phase stability tested. The design of this oven is described in section 6.2.

Laser transmitter, receiver and phase detector as well as several other system components are temperature sensitive. Temperature stabilization is required to remove errors induced by ambient temperature changes. In the final system the oven 2 will be used for this purpose. Required oven temperature stability is $<0.5^{o}$C over +10 to $+30^{o}$C ambient temperature range.

During laboratory system tests temperature stabilization of the entire system was realized by the use of a large climate chamber.

5.11. OPTICAL LOSS

Optical power loss is a very important issue in the FO link. Summary of optical loss of system components is shown in figure 5.11. Two optical signal paths from the laser to the F.O. receivers can be distinguished:

1. Leading through the entire system, and reflected by the mirror back through long link, phase shifter and circulator to F.O. receiver A.
2. Leading through the entire system up to directional coupler and F.O. receiver B.

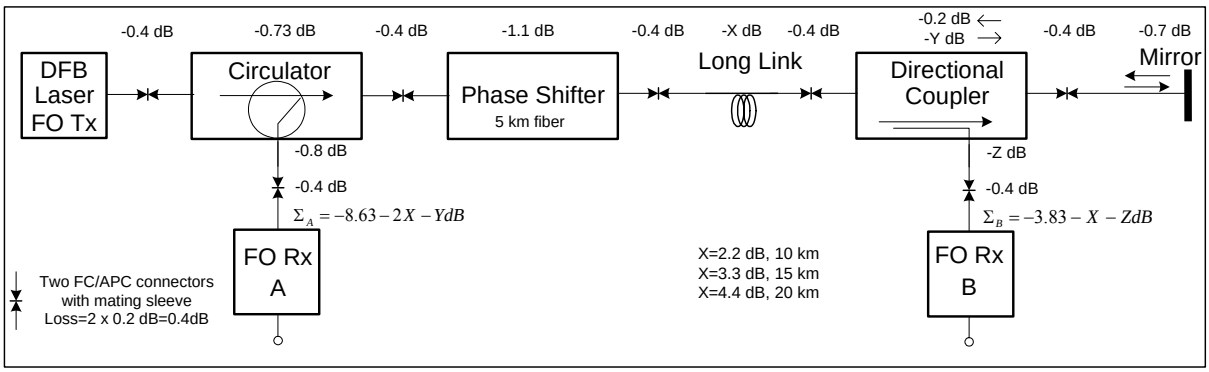

Fig.5.11: *Optical loss in the system*

The Spinner F.O. receivers operating input power level range is between -15 dBm and +3 dBm. The laser transmitter output light power is +2 dBm (RMS) (possible adjustment to +4 dBm) so the optical loss to each receiver should not exceed -18 dB and advisable is 2-3 dB safety margin.

Several lengths of long link fiber and directional coupler types were considered. Therefore in table 5.11 the optical loss was given for different combinations of these components.

Table 5.11: Optical loss in the system

Path to	**To Rx A [dB]**			**To Rx B [dB]**		
Link length/ Coupler Type att.	10 km X=2.2 dB	15 km X=3.3 dB	20 km X=4.4 dB	10 km X=2.2 dB	15 km X=3.3 dB	20 km X=4.4 dB
50/50,Y=4 dB, Z=4 dB	17.03	**19.23**	**21.43**	10.03	**11.13**	**12.23**
30/70,Y=2 dB, Z=6 dB	15.03	17.23	**19.43**	12.03	13.13	**14.23**
20/80,Y=1.3 dB, Z=8.2 dB	14.33	16.53	**18.73**	14.23	15.33	**16.43**

The cases where optical loss exceeds 18 dB were marked with red bold font. If one path can not be used then of course second path also must be excluded therefore corresponding path B values were marked too.

The conclusion is that the long link length should not exceed 15 km and the optimal coupler type is 20/80 because of almost equal losses in both signal paths what gives same operating conditions of both receivers. Nevertheless, measurements were performed with 20 km of fiber – such spool was also available. System operation was achieved but on the threshold of the sensitivity of the FO Rx A. Achieving phase lock was possible beacue values shown in the table 5.11 and figure 5.11 are given for the worst case. In the case of necessity of building such long connections in the final system a laser module with higher output power must be used to ensure continuous system operation.

6. SUBSYSTEM DESIGN ISSUES

6.1. TEMPERATURE CONTROLLED OVEN 1

This device was originally intended to work as an optical phase shifter with spool of fiber inside (see section 5.6). After manufacturing and tests of oven 1 an improved oven no. 2 was designed using new components available on the market. Measurements results from both ovens (see section 8) show that oven no. 2 is slower in changing temperature but much more stable. At beginning stages of system controller development a phase shifter (stable against ambient temperature) was required (not an issue in the final design). Therefore the oven 2 was used for the phase shifter purpose.

It must be also mentioned that the term "oven" is not exactly precise because both devices can be used to both: heat and cool. They should be called "climate chamber" but for simplicity "oven" name is used in the whole document.

Requirements and concept

Required:

- min ~30°C temperature range (+10°C - +40°C)
- chamber big enough to hold spool with fiber - 35cm x 35cm x 20cm
- external temperature control input – by applying voltage in the range 0-10V
- internal temperature control (for example by precise variable resistor)
- PI or PID temperature controller
- internal thermometer

Electronic circuit description

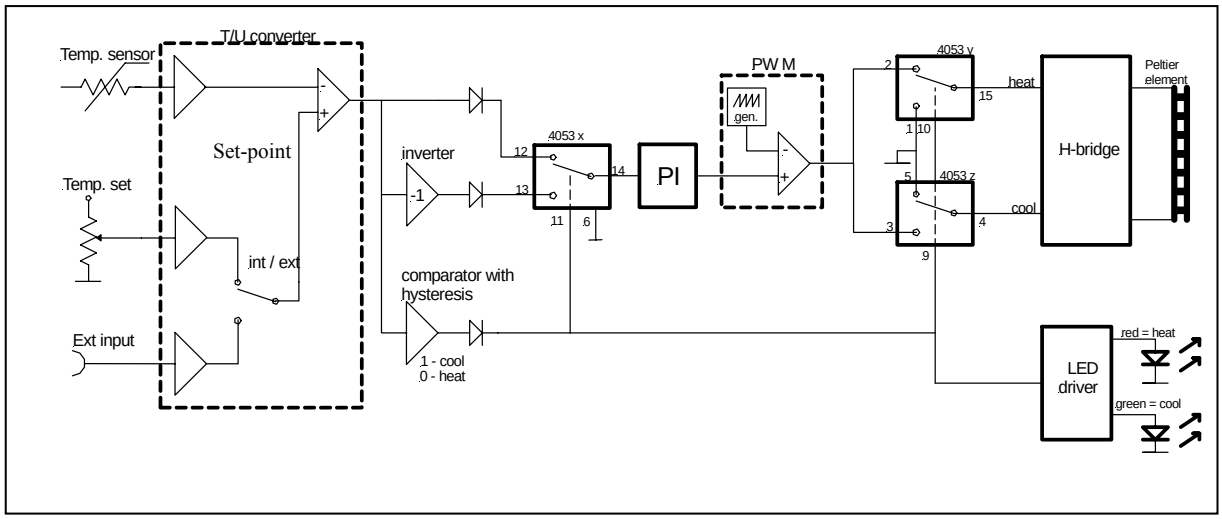

Figure 6.1.1: *Block diagram of oven 1.*

Design has been based on:

- high power thermo electric cooler (TEC), air-to-air type manufactured by Melcor
- 19" type box with thermal insulation
- self developed PI temperature controller
- LED thermometer with ICL7107 circuit

Oven 1 block diagram is shown in figure 6.1.1. Most important elements can be distinguished: temperature to voltage converter (T/U), heat/cool switch, PI controller, pulsed width modulator (PWM) and TEC with high power H-bridge drive.

Temperature sensor and precise amplifier circuit are used to convert temperature value into voltage. Obtained voltage value is then subtracted from the set-point voltage. Either internal set-point voltage produced by a precise 10-turn potentiometer can be used or external voltage can be provided via the external input. A comparator circuit is used to detect whether internal oven temperature is lower or higher than set-point temperature and to control current direction in the TEC element. Heating or cooling inside of the oven chamber is obtained depending on the TEC current direction. After passing a simple analogue switch (4053 type) control voltage is given to the PI controller. Result of multiplication by constant gain factor P and integration result multiplied by factor I is added to produce voltage given to the PWM (Pulsed Width Modulator) circuit. There current pulses are generated with duty cycle proportional to the PI controller output voltage value. High power H-bridge drives the TEC.

The LED driver block is used to switch between the red LED when the TEC element is heating and the green LED when the TEC cooling.

Additionally a commercial thermometer module with LED display on the front panel of the oven is used for visual monitoring of the oven temperature.

Detailed schematic diagrams can be found in Appendix A.

Oven 1 photographs

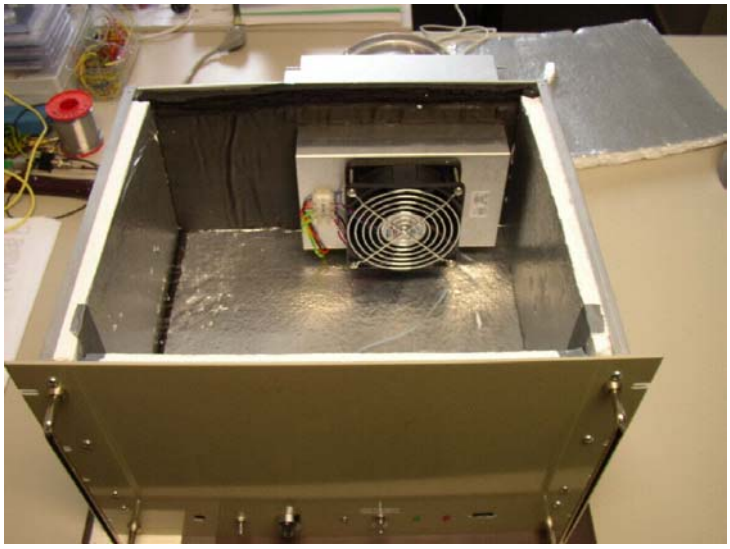

Figure 6.1.2: *Oven 1 chamber.*

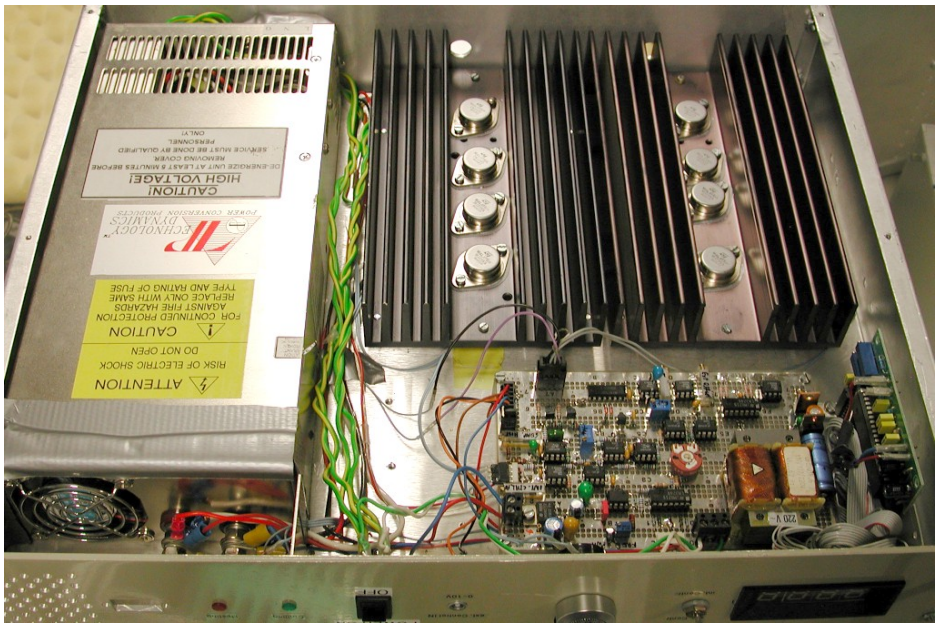

Figure 6.1.3: *Oven 1 electronics*

Figure 6.1.4: *Oven 1 front panel*

In figure 6.1.2 the oven chamber with thermal insulation and the TEC is shown. Oven electronics was developed as a prototype using standard easy available components. The layout of electronic components in the electronic chamber (figure 6.1.3) was designed in such a way that there is airflow aroung high power heatsink forced by the power supply fan. Test results and optimization procedure description can be found in the section 8.1

6.2. TEMEPRATURE CONTROLLED OVEN 2

The oven 2 was designed after gaining experience with oven 1. It is used for the purpose of optical phase shifter. Phase of the optical signal is changed by heating or cooling a spool of fiber inside the oven (described in section 4.1). The use of commercial modules for this oven significantly simplified design and improved device performance in comparison to oven 1.

The design is based on the Thermoelectric Cooler (TEC) manufactured by Telemeter, the HTC 1500 temperature controller (Wavelength Electronics) and the AMC 30A8T PWM servo amplifier.

Maximum current for the TEC is 11.5A and heating or cooling is obtained by changing the current direction. Therefore the TEC element is driven by PWM module with a high power H-Bridge CMOS output (AMC servo amplifier).

Digital thermometer module with LED display is used on the front panel of the oven for visual monitoring of the oven temperature.

Oven 2 block diagram is shown in the figure 6.2.1.

The principle of work of oven 2 electronics is similar to oven 1 but most components are integrated inside commercial modules. Text below describes details concerning the use of those modules in the design.

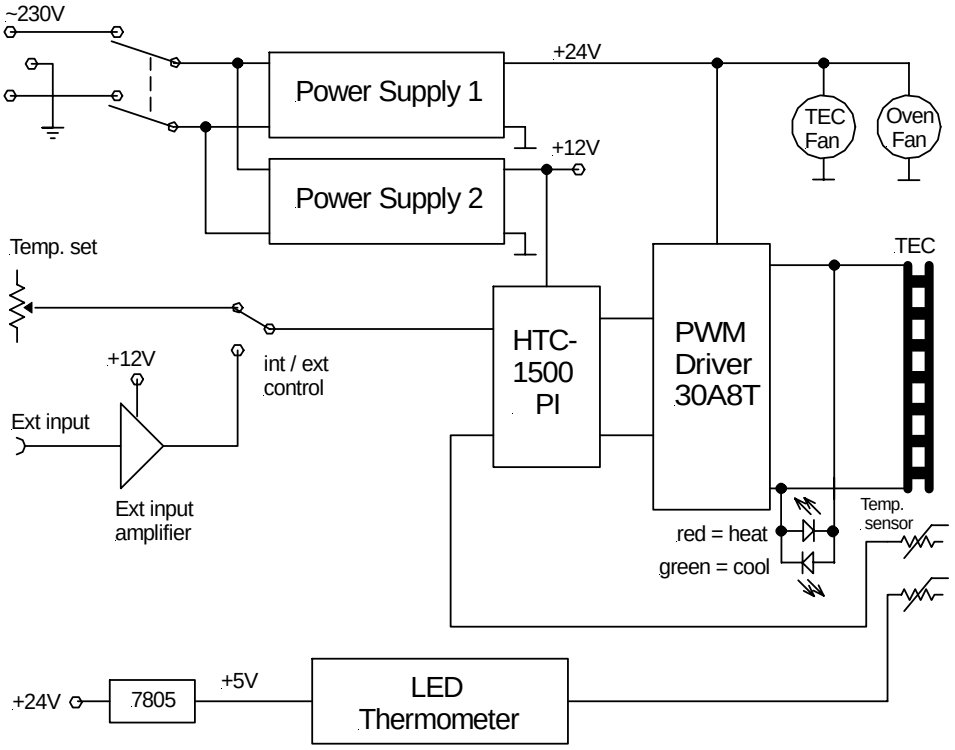

Figure 6.2.1: *Oven 2 block diagram*

The temperature controller

Hybrid, PI type HTC-1500 temperature controller has been used. Only several external components are required for proper operation.

The device is destined to work with TEC elements with operating current up to 1.5 A which is below the Telemeter TEC module current (11.5 A). Therefore the HTC controller is followed by the PWM driver (described in the following text) and it operates at a very small current required to obtain the control voltage for the PWM driver.

The HTC-1500 circuit diagram is shown in the figure 6.2.2.

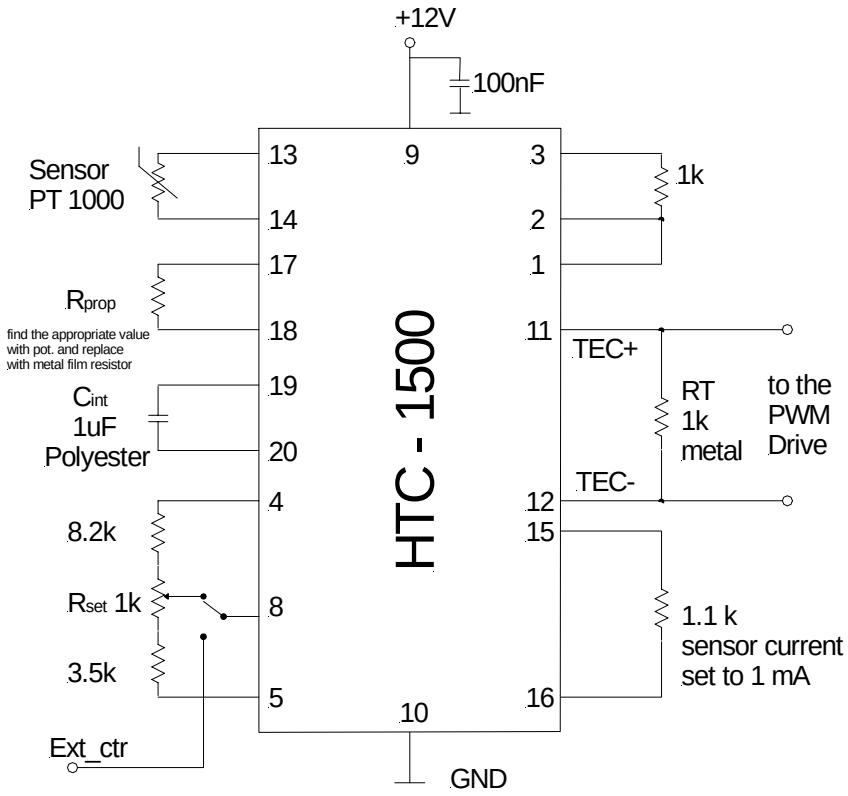

Figure 6.2.2: *The HTC-1500 circuit.*

Circuit description

1. Output current bias: pins 2 and 3 shorted for bipolar operation (heating or cooling).
2. Output current limit: 200 mA with 1 kΩ resistor between pin 2 and pin 3.
3. Sensor bias current: 1 mA with 1.1 kΩ resistor between pin 15 and pin 16.
4. Sensor: PT1000, RPT=3.85*T[^{o}C]+1000.
5. Proportional gain: can be adjusted between 1 and 100 by 500 kΩ potentiometer inserted between pins 17 and 18. The potentiometer has been replaced by metal film resistor after finding the appropriate value.
6. Integrator time constant: set to 1 second by 1 μF capacitor between pins 19 and 20. The polyester type capacitor was chosen because of good temperature stability.
7. Output: pins 11 and 12. 1 kΩ resistor connected. The voltage drop on this resistor is used to control the PWM driver input.
8. Temperature set-point: The oven temperature can be controlled internally by 1 kΩ potentiometer and externally with voltage between 0 and 10 V. The table below includes the resistance and the voltage produced by the PT1000 temperature sensor at three operating temperatures:

Temp. [^{o}C]	R_{PT} [Ω]	V_{PT} [V]
+5	1019	1.019
+50	1192	1.192
+80	1308	1.308

It was intended that internal control provides temperatures between +5 and +80 °C (more than required but the TEC capability can be used if needed), and the external control operates between +5 and +50 °C. The low temperature limit is set because at temperatures close to 0 °C and below, water and ice settle inside the oven. When used in the feedback loop for the fiber optic system the operating temperature range of 30 °C is sufficient but +45 °C (+5 to +50 °C) is set to have a safety margin.

The temperature set-point voltage (for internal control) is obtained by dividing the 3.675 V reference from the HTC-1500. Two resistors (8.2 kΩ and 3.5 kΩ) and 1 kΩ potentiometer have been used to provide voltages between 1.019 V and 1.308 V. The external input should also provide voltages in this range but for easier use a voltage level converter is used (figure 6.2.3) to accept external control voltages in range 0V to 10V.

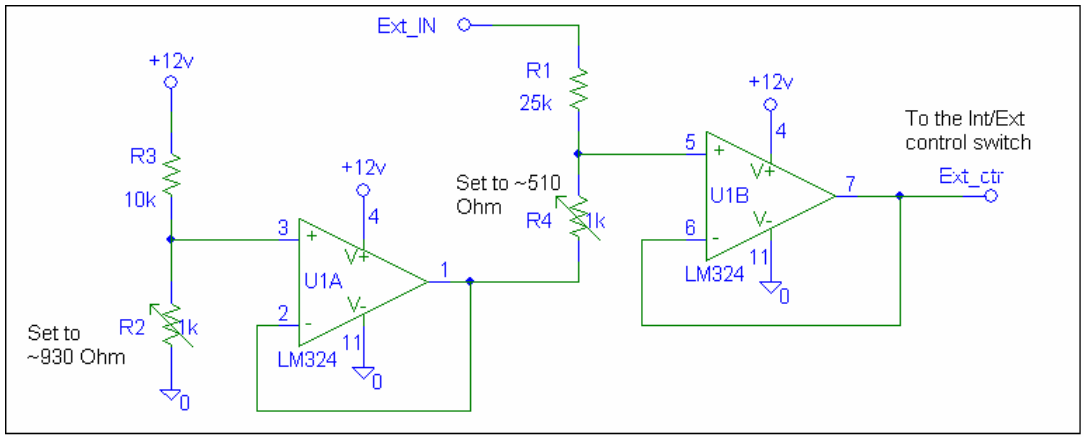

Figure 6.2.3: *External input circuit.*

The AMC servo amplifier:

The device was designed for brush type motors control but it may be used as a current driver for the thermoelectric cooler.

Main features:

- DC supply voltage 20 – 80V,
- peak current 30A,
- maximum continuous current 15A,
- minimum load inductance 200µH,
- full over-current, over-voltage, over-heating and short circuits protected,
- internal MOSFET H-bridge drive,
- internal PWM circuitry.

Switch setting

The operating mode of AMC drive is programmed by 10 switches. In this application switches are set as in table below:

SWITCH	SETTING	FUNCTION
1	OFF	Internal voltage feedback
2	OFF	IR compensation
3	OFF	Current loop gain
4	OFF	Current loop integration

5	ON	No current scaling
6	OFF	Cont./Peak current ratio 50%
7	OFF	Current loop integrator operating
8	ON	Shorts voltage loop integrator capacitor
9	OFF	Disabled if SW8 is ON
10	OFF	Offset sensitivity decreased

Potentiometer setting

NO.	SET	DESCRIPTION
POT 1	Maximum CCW	Gain decreased
POT 2	Find max. current	Current limit
POT 3	Maximum CW	Reference gain equals 0.5
POT 4	N/A	

Pin description

There are two connectors (P1 and P2) in the AMC device. The 4-pin P2 is a high power connector used for the power supply and the MOSFET driver output. The use of pins of connector P1 in this application is described in the table below.

PIN	NAME	DESCRIPTION
1	+10V OUT	Used to obtain +5V
2	SIGNAL GND	Used to obtain +5V
3	-10V OUT	Not used
4	+REF IN	connected to the temp. controller output
5	-REF IN	connected to the temp. controller output
6	-TACH IN	Not used
7	+TACH	Not used
8	CURRENT MONITOR OUT	Not used
9	CURRENT REFERENCE OUT	Not used
10	CONT. CURRENT LIMIT	Not used
11	INHIBIT	Turns the “H” bridge ON (+5V)
12	+INHIBIT	+ current direction enabled (+5V)
13	-INHIBIT	- current direction enabled (+5V)
14	FAULT OUT	Not used
15	SYNCH IN	Not used
16	SYNCH OUT	Not used

The schematic diagram of the AMC device circuit is shown in figure 6.2.4. Inductances connected in series with the TEC module provide minimum load inductance required by the servo amplifier.

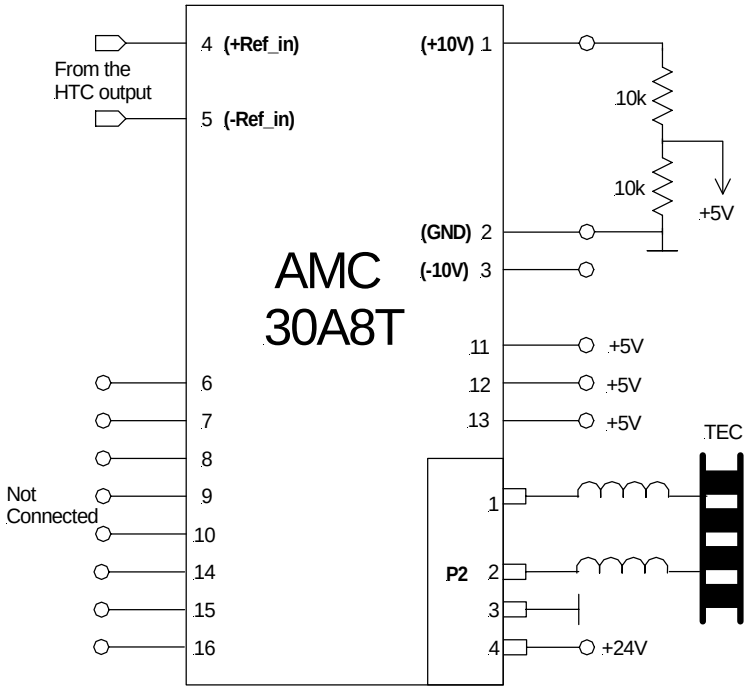

Figure 6.2.4: *The AMC servo amplifier circuit.*

Oven 2 photographs

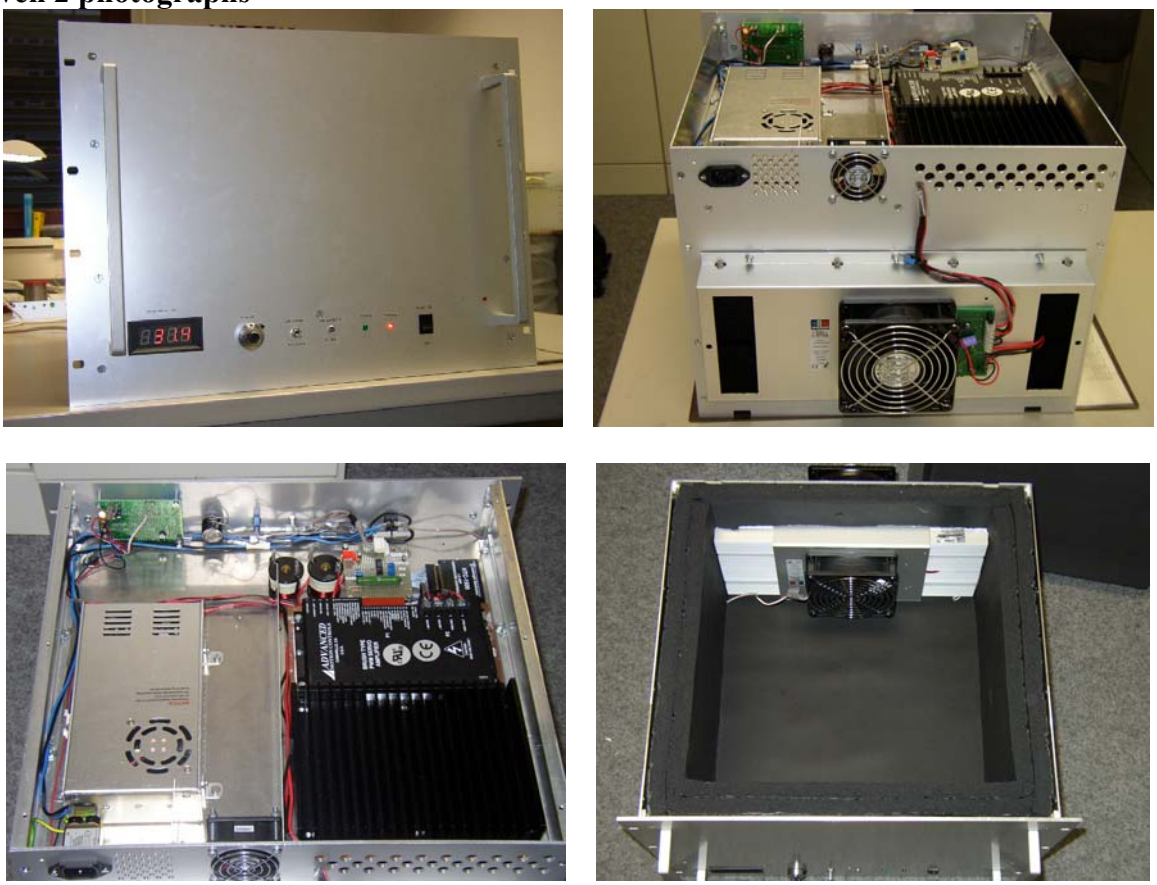

Figure 6.2.5: Oven *2 front panel, back, electronics and temperature isolated chamber.*

A double thermal insulation has been used in the oven 2 to obtain higher internal temperature stability when ambient temperature changes. Special aluminum walls have been designed and additional fan has been used in the oven 2 electronics chamber to insure good airflow over high power electronic components

Oven 2 performance tests are described in section 8.2.

6.3. LASER TRANSMITTER

The Agere D2502G type 1550 nm laser module is used. The module contains: laser diode, pin type photo diode for automatic laser power control, TEC element and 10kΩ thermistor for controlling the laser temperature.

Main design assumptions:
- the bias current is controlled by the MAX3263 laser diode driver with Automatic Power Control (APC);
- laser temperature is regulated by the HTC 1500 temperature controller;

Bias current control circuit with MAX3263:

The measurement results provided by laser module manufacturer show the laser output power and monitor diode current vs. laser diode current. The maximum measured power is 4 mW. Here it has been assumed that the laser module provides **2 mW** of optical power.

The laser diode current = 33.45 mA
The monitor diode current = ~280 μA

The MAX3263 driver is used here to control only the bias current. Therefore pins OUT+ and OUT- (refer to device datasheet) are not connected to the diode and remaining internal blocks are disabled or operated at minimum current.

The laser diode must be biased with negative voltage. Therefore the VCC pins of MAX3263 are connected to ground and GND pins are connected to -5V.

Below the use of MAX3263 pins is described:

For element names see figure 6.3.1.

Pin 2: IPINSET; This pin is used for programming the monitor photodiode current. The photodiode current in used device is 280 μA. From typical operating characteristic of MAX3263 a value of R_{PINSET}=5.6 kΩ was derived.

Typical current value of the D2502 monitor diode is 1 mA but it may be between 0.1 and 2 mA, when laser output power is 1 mW. The IPIN input of the MAX3263 can operate with currents up to 1 mA (absolute maximum 2 mA). Therefore the monitor current of other laser modules may exceed the limit. Additional, stable, constant current sink connected in parallel with IPIN has been foreseen to sink part of diode current and prevent IPIN output from damage.

After turning APC on the laser diode current is controlled automatically and its value depends on the PIN diode bias current. Therefore precise value of R_{PINSET} should be found experimentally after turning the APC on.

Pin 3: FAILOUT; This output is used to indicate when the laser diode bias current control is out of regulation (LOW state appears on this output). The pin is connected to VCC (GND here) via 2.7 kΩ. The LED diode connected to this output indicates laser failure on the transmitter front panel.

Pin 4, 7, 17, 19, 21: GND; MAX3263 ground. Connected to -5V!

Pin 5, 6: VIN; not used, connected to -5V

Pin 8: VCCB; GND

Pin 9: ENB-; -5V

Pin 10: ENB+: GND

Pin 12: OSADJ; connected to VREF by 10 kΩ resistor. The value is taken to minimize current consumption. There is no modulation current provided from MAX3263

Pin 13: IBIASFB; connected to IBIASSET

Pin 14: IBIASSET; connected to VREF via resistor. The automatic power control (APC) can correct the current 40 mA up or down from the bias set. The maximum value should not exceed 75 mA. So the bias current should not be higher than 35 mA. RBIASSET value is 1.8 kΩ connected in series with 10 kΩ variable resistor.

Pin 15: IMODSET; modulation driver is not used. Therefore this current is set as low as possible with 10kΩ resistor.

Pin 16: IBIASOUT; connected to bias input of the laser module. Optional RC shunt filter has been foreseen but not applied.

Pin 18, 20: OUT; not used, shorted by 10 kΩ resistor.

Pin 23: IPIN; connected to the monitor diode. Optional current sink has been foreseen but not applied. See pin 2 description.

Pin 24: SLWSTRT; connected to -5V by 1 nF capacitor gives 25μs start time.

Temperature controller circuit

The HTC1500 hybrid temperature controller is used to keep laser temperature at +25 ^{o}C. A schematic diagram is shown in the figure 6.3.1.

- +5V power supply gives output voltages satisfying the TEC (integrated in the D2500 laser module) requirements;
- output current limited to 600 mA by 4.4 kΩ resistor connected between pin 1 and pin 2;
- sensor bias current set to 100 μA in by resistor R_8=12.1 kΩ.
- integrator time constant set to 1 second by 1 μF polyester capacitor
- Temperature set-point is set to 25^{o}C (set-point voltage equals 1 V) by two resistors or adjusted by 10kΩ variable resistor connected to V_{refout} pin;

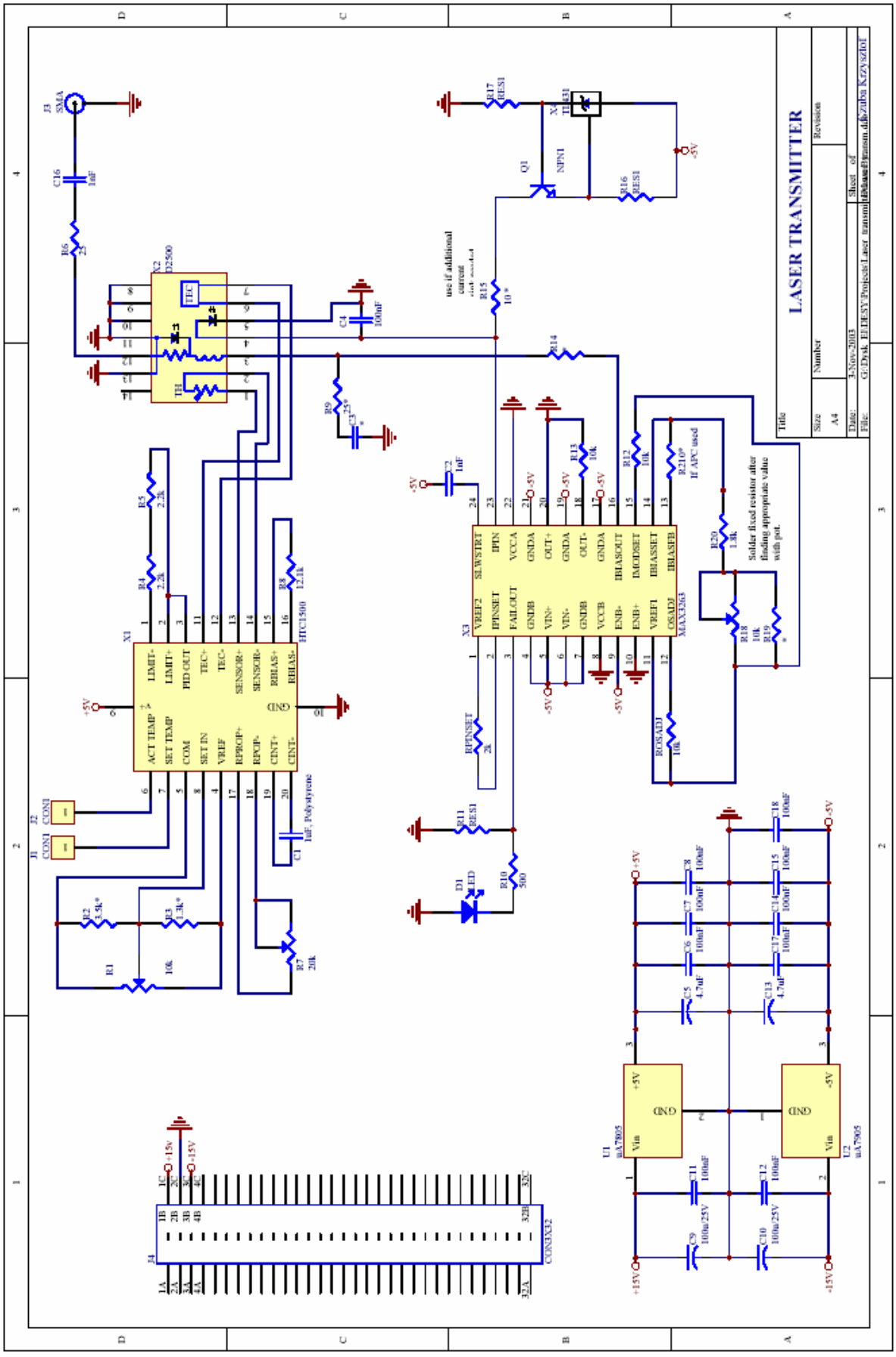

Figure 6.3.1: *Laser transmitter schematic diagram*

Power consumption:

The power supply for the laser module is +/- 15V. Voltages are internally regulated down to +/-5V.
Laser diode: ~35 mA (-5V)
Laser driver ~20mA (-5V) – monitor diode + internal circuits
Temperature controller + laser TEC – 250 mA (+5V) but TEC current may reach 600 mA in extreme conditions.

Circuit adjustments:

1. Before switching power ON!!: Set bias current potentiometer (R_{18}) to resistance that together with R_{20} (1.8 kΩ) assures required bias current. Total resistance value can be found in the MAX3263 datasheet. In the case of used laser module it is about 1800 – 1900 Ω.
2. Do not solder R_{21} –the automatic power control (APC) will be switched off.
3. Set proportional gain of the HTC 1500 controller to value between 20 and 30 (works properly, higher gains not tested) by setting R_7 to ~12 kΩ.
$$GAIN = \frac{500k\Omega}{R_7 + 5k\Omega}$$
4. Set laser temperature to ~25°C if a potentiometer (R_1) is soldered instead of fixed resistors (R_2 and R_3).
5. Now one can switch power on for the first time.
6. Measure laser diode current (voltage at R_{14}=1 Ω) and adjust precisely (by R_{18}) to a value that gives 2mW of light power. Current values and other data is provided by laser manufacturer for every module.
7. Measure temperature controller voltages – set and actual monitor pins on the board. Should be about 1V.
8. Solder R_{21} to switch the APC on and measure laser current again.
9. If laser diode current differs significantly from expected value adjust R_{PINSET} experimentally.
10. Measure optical power.

Mechanical design:

Laser transmitter modules have been assembled on EURO size (160 x 100 mm) printed circuit board. Heat-sink is added with sufficiently low thermal resistance to distribute the dissipated power. Picture of designed laser module was shown in the figure 6.3.1.

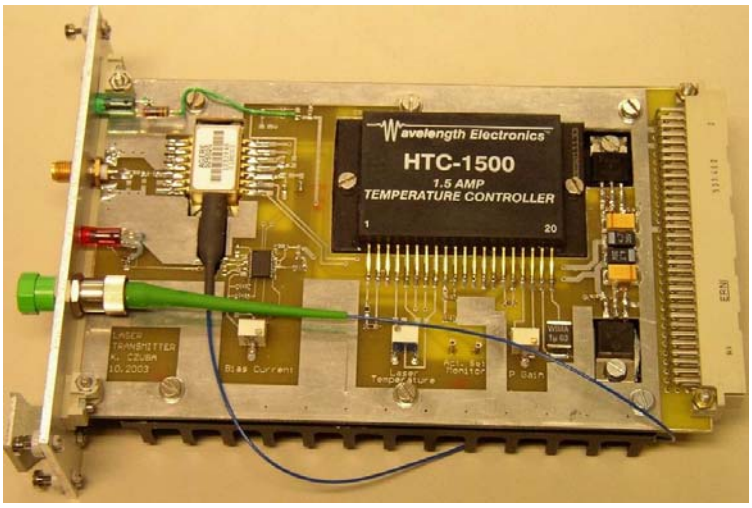

Figure 6.3.1: *Laser transmitter board*

6.4. PHASE DETECTOR CIRCUIT

The HMC403 large range digital phase detector (by Hittite company) chip has been used for the first system tests. Printed circuit board with necessary analogue circuits (designed by Henning Weddig) has been manufactured as shown in figure 6.4.1.

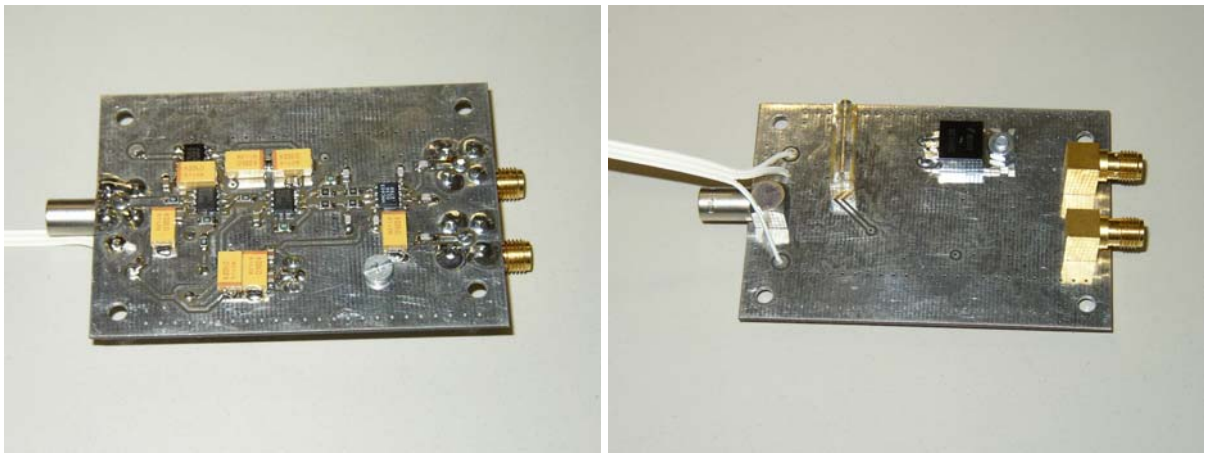

Figure 6.4.1: *Phase detector board*.

The most important feature of this phase detector is that it can operate directly at frequency 1.3 GHz. Therefore there is no need to use down-converter and the FO system is significantly simplified comparing to a scheme with down-conversion. Sources for additional phase errors caused by additional mixer (in case of down-conversion) and LO frequency generator are avoided. Two RF signals in power range -10 dBm to +10 dBm should be provided to phase detector inputs.

Another advantage of this type of phase detector is large measurement range – 360^{o} in comparison with multiplier type phase detectors (180^{o} full scale only).

6.5. OTHER SYSTEM COMPONENTS

Several commercial components are used in our system. Following figures show pictures of those components. Parameters and most important issues are given in chapter 5. A plastic

cover of the fiber spool (see figure 6.5.4) was found to be a good thermal insulation which slows the phase shifter down.

Figure 6.5.1: *Fiber-optic circulator.*

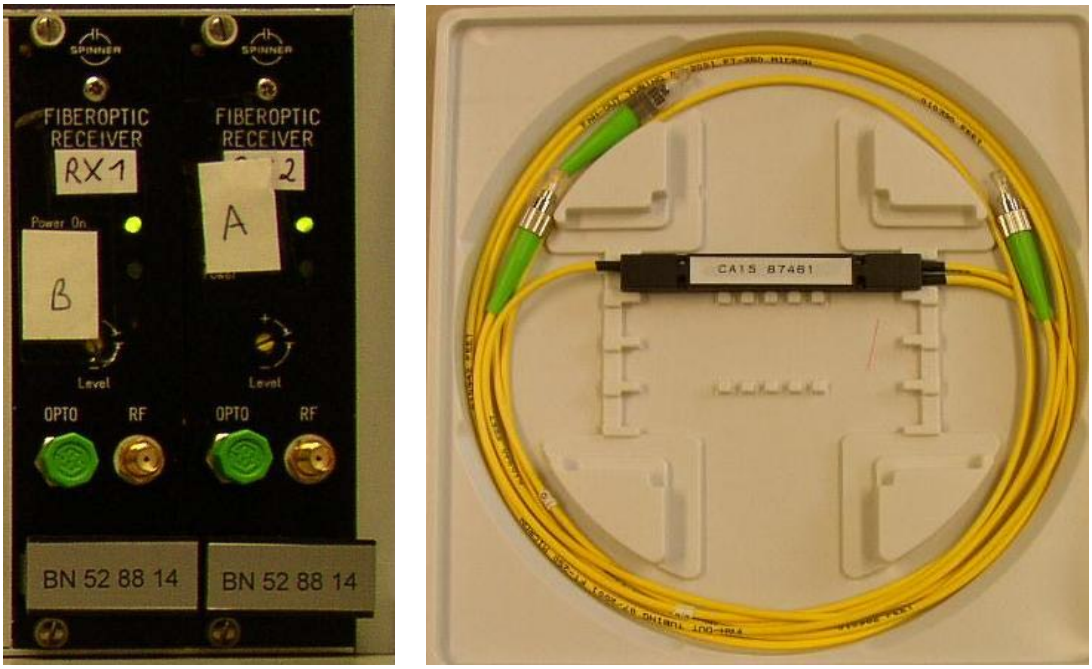

Figure 6.5.2: *Analogue (2.5 GHz bandwidth) receivers and fiber optic directional coupler.*

Figure 6.5.3: *Adjustable fiber-optic mirror.*

Figure 6.5.4: *Spool with fiber (5km and 20km).*

7. SYSTEM CONTROLLER DESIGN

7.1. OVERVIEW

Development of the system controller was the biggest part of work performed while building the FO system prototype. Therefore a separate chapter is dedicated to this controller.

The purpose of the system controller is the real-time phase stabilization of the signal at the end of the long fiber optic link. The target device module should be as simple and as cheap as possible and easy to configure and to install in the accelerator environment. A study of different system controller methods and their realization led to the following plan for the controller realization:

1. Development of a digital controller prototype in a convenient environment. A PC with Matlab® connected to a real-time data acquisition card can be used. This way it is possible to use all features of the computer software like plotting, saving and other operations on measured data.
2. Conversion of developed Matlab algorithms to (e.g.) C programming language code.
3. Development of stand-alone microprocessor board with necessary AD and DA converters. Use of prepared C code.

The following description in this chapter concerns mainly point 1,because points 2 and 3 have not been realized at this stage of the project. A Graphical User Interface (GUI) in Matlab provides many features for the system development. These features are: possibility of plotting measured data, applying different controller equations, different methods for finding controller equation parameters and several numerical integration methods. This way it is easy to make performance tests and compare the results to find the best method.

Since the accelerator tunnel temperature changes relatively slow - rather long time process, e.g. $1^{o}C$ per hour - a very slow measurement device is sufficient for the system controller. There seems to be no need to use data acquisition devices with a sampling rate higher than 1 sample per second.

The work was started with AD-USB4 device (manufactured by the Voltcraft company). It is an easy to use USB data acquisition device. Unfortunately, after first measurements several disadvantages of the AD-USB4 for the FO system were found and it was replaced with a microcontroller based data acquisition board. In the future this microcontroller device can be

successfully used for standalone system operation. This solution has the advantage that the same hardware will be used for development and for the final product.

In the following text the controller principle, the features of our GUI and the microcontroller board are described.

7.2. PID CONTROLLER

Feedback controllers are commonly used to automatically adjust a variable to some set-point with assumed accuracy. One of basic controller types is the PID controller. PID stands for proportional-integral-derivative. The set-point is the desired measurement result. The difference between set-point and measurement result is called error signal (term 'error voltage' is used in the following text). See figure 7.2.1 for a basic PID controller feedback system block diagram. The "s" parameters correspond to the Laplace transform domain. A detailed analysis of PID feedback systems can be found in multiple references e.g. [4]. It should be mentioned here that the proportional gain (P) reduces the error voltage but the use of too high P leads to system instability. Controllers with proportional gain only cannot reduce the error voltage to zero. The integration part with I parameter is used to remove the error. Additionally the derivative component D is used to improve stability and response (e.g. minimize overshoot).

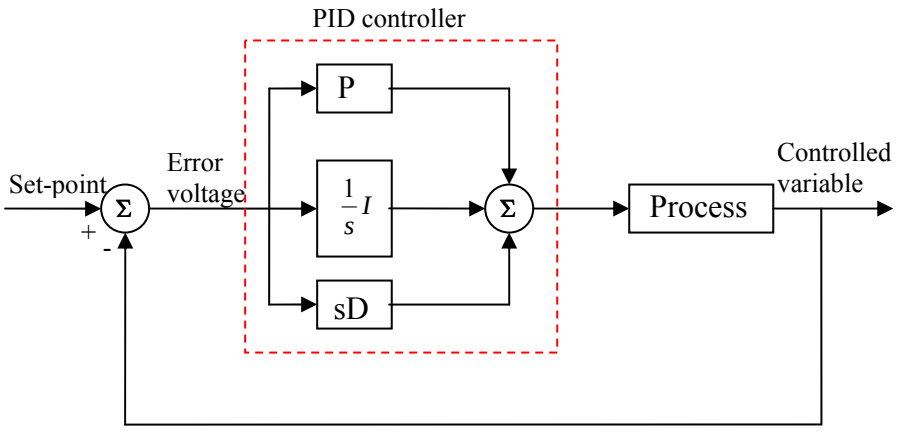

Figure 7.2.1: *Feedback control loop with a PID type controller.*

The PID controller can be realized in different ways e.g. analogue electronic circuits. In this application a digital PID controller is realized using numerical methods for integration, derivation and summation. This way, large flexibility in modifying controller parameters is obtained and errors that are characteristic for analogue circuits are avoided.

7.3. CONTROLLER SOFTWARE

GUI

A Graphical User Interface (GUI) was developed in Matlab to simplify the controller parameter calculation and tests. The GUI surface is shown in figure 7.3.1. The software includes:

- 6 channel measured data plot window with channel selection
- PID controller module with configurable parameters
- Phase error measurement display

- Long link simulator control – values and duration of temperature changes of the long link simulator (20 km of fiber inside oven 1) can be programmed and executed automatically.

Additional GUI features can be accessed using the GUI menu (see figure 7.3.2.):

- System simulation utility by Simulink.
- Controller parameter calculation utility –P, I and D values can be calculated after measurement of the system response. Several calculation methods were implemented: Cohen Coon [4, 5], Takahashi (method 1) [4, 6], Takahashi (method 2), Least Squares [7]. The PID calculation sub-GUI is shown in figure 7.3.3.
- The choice of numerical integration method. Four methods are implemented: rectangle [6], trapeze [8], Simpson and Romberg method [9].
- Automatic measurement statistics calculation, like system short and long term stability.

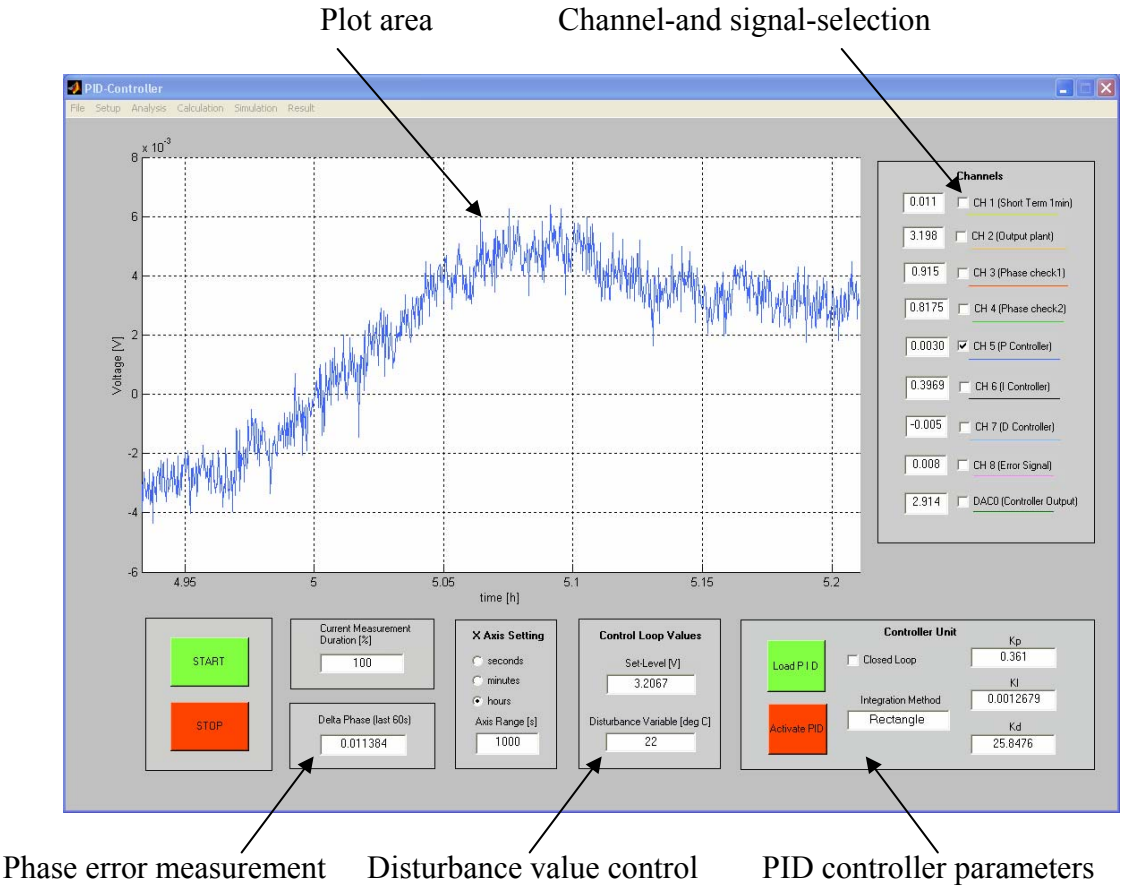

Figure 7.3.1: *GUI surface.*

Figure 7.3.2: *Menu of the GUI.*

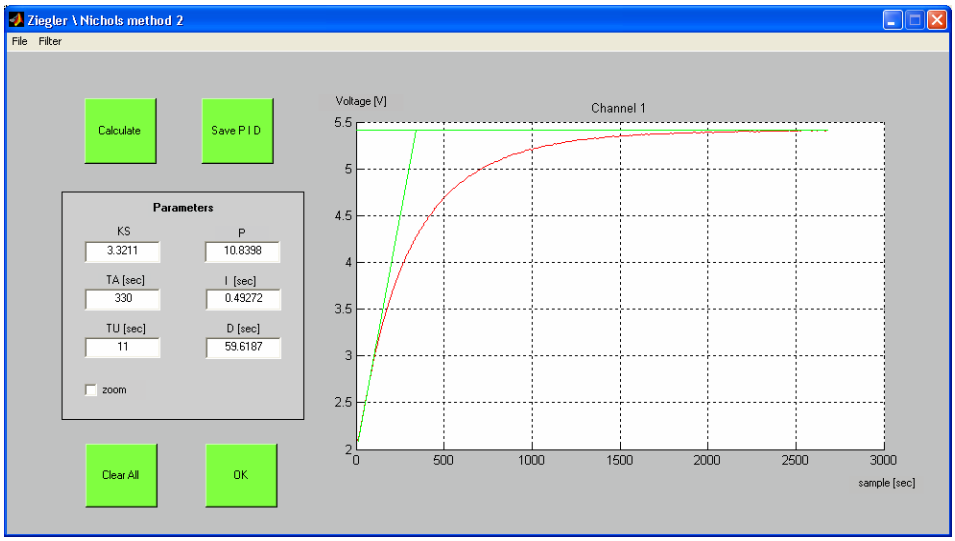

Figure 7.3.3: *Controller parameter calculation utility.*

7.4. CONTROLLER HARDWARE

A data acquisition module with analogue-to-digital (ADC) and digital-to-analogue (DAC) converters is used as the interface between the controller software (PC) and the fiber optic system – as it was mentioned in section 7.1.

The MSC1211 type microcontroller is used. It integrates in one chip the 8051 microprocessor core, ADC and DAC with adequate parameters for our purposes. Most important MSC1211 features are:

- 8 channel 24-bit ADC
- Four 16-bit DACs
- Two serial ports
- 32k of flash memory
- 32-bit accumulator
- High-speed SPI or I^2C interface
- 16-bit PWM output
- 1,280 bytes of data RAM

The system development was started with the MSC1211 evaluation board which allows an easy start and development of design ideas before creating the final device. The picture of the MCS1211 evaluation board is shown in figure 7.4.1.

Figure 7.4.1: *MSC1211 evaluation board.*

The Liquid Crystal Display (LCD) was connected to the board for easier software debugging and easier device interfacing. Serial port communication with a PC and the Matlab GUI was established – see figure 7.4.2 for a system block diagram.

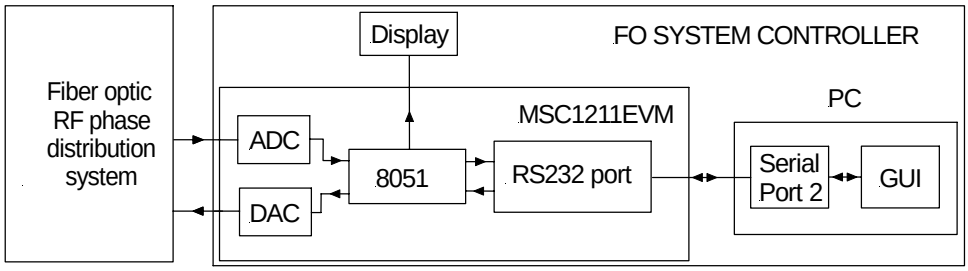

Figure 7.4.2: *Fiber optic system controller block diagram.*

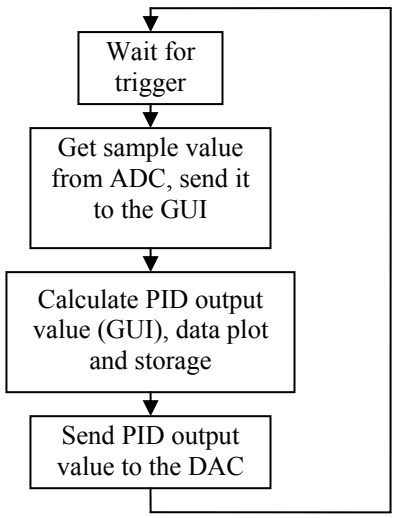

Figure 7.4.3: *Data flow in the FO system controller.*

A C language program was written and compiled for the MSC1211 microcontroller for communication with the GUI and data acquisition. The data flow in the FO system controller is depicted in figure 7.4.3. As mentioned before, the MSC1211 board has been used in the first stage of the project only as a data acquisition device. All PID controller calculations are implemented in the Matlab code. In the future, after finding satisfying PID controller parameters, developed Matlab equations will be converted into the C language and the MSC1211 will be operating as standalone PID controller. An auto-tune mode for the controller is also planned, so the device can adapt to new system configurations. The end stage of development of the PID controller will be the design of a PCB for the MSC1211 – the evaluation board is not a target device.

8. SYSTEM COMPONENT TESTS

8.1. OVEN1 PERFORMANCE TESTS

This chapter describes measurement of parameters of the oven designed for the optical phase shifter purpose – as described in chapter 6.1. Several tests were performed to verify oven parameters. Some of them result in the conclusion that further improvement is required. Below, the most important tests are described:

8.1.1. Measurements of oven responses for step changes of temperature

Objective: Check the oven performance with I (Integral part) of the PI controller disabled

Procedure:
Disabled I section in the PI controller.
Rise time and overshoot measured for several P (controller proportional gain) values
Resistor numbers correspond to schematic diagrams in the appendix 1.

1) P gain set to 28 (R_{17}=6k). Obtained rise time equals 9 minutes. No overshoot.

2) P gain set to 32 (R_{17}=7k). Obtained rise time equals 6.5 minutes.

3) P gain set to 36 (R_{17}=8k). Obtained rise time equals 5 minutes. Little overshoot – 0.5 ^{o}C.

4) P gain set to 68 (R_{17}=15k). Rise time equals 5 minutes. Overshoot – 1.8 ^{o}C.

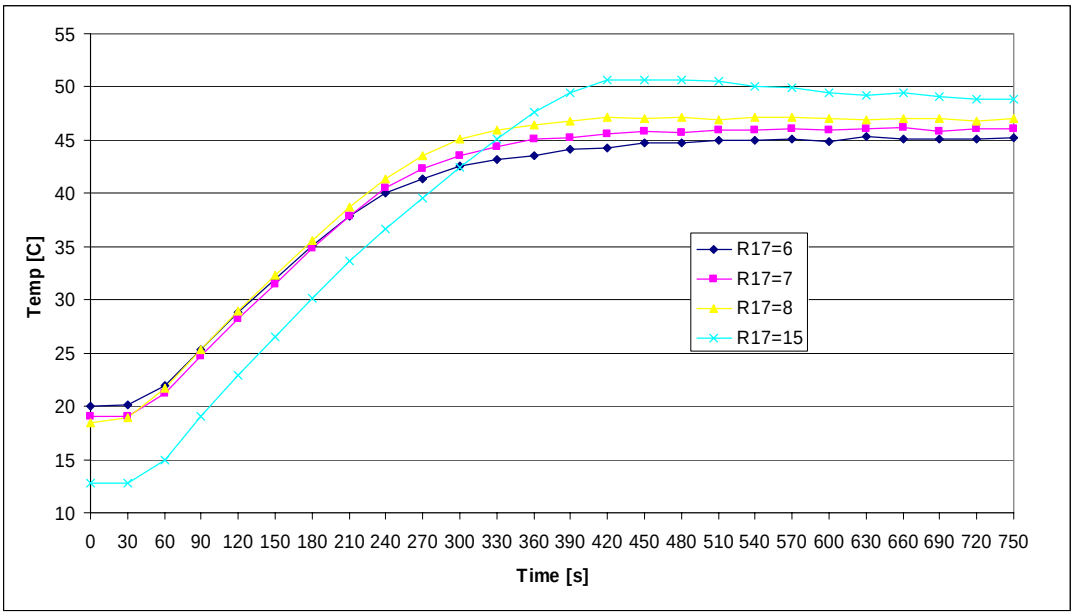

Figure 8.1.1: *Oven temperature rise for various controller proportional gain value.*

Conclusions:

The higher gain the higher temperature when heating and lower when cooling – obvious: the feedback operates with smaller error voltage. Overshoot is observed with gain of 68.

I parameter of the PI controller is required to increase rise time and remove the steady state error

8.1.2. Oven 1 temperature stability versus ambient temperature

Objective: Find oven temperature dependence on the ambient temperature.

Procedure: A commercial data acquisition device (iDAQ) was used to measure temperatures inside the oven, outside of it and also the temperature of the air blown out of the electronic chamber by the power supply fan. During this measurement the climate chamber was unavailable, therefore the random office temperature changes were used for tests.

The P gain set to 32.

Results:

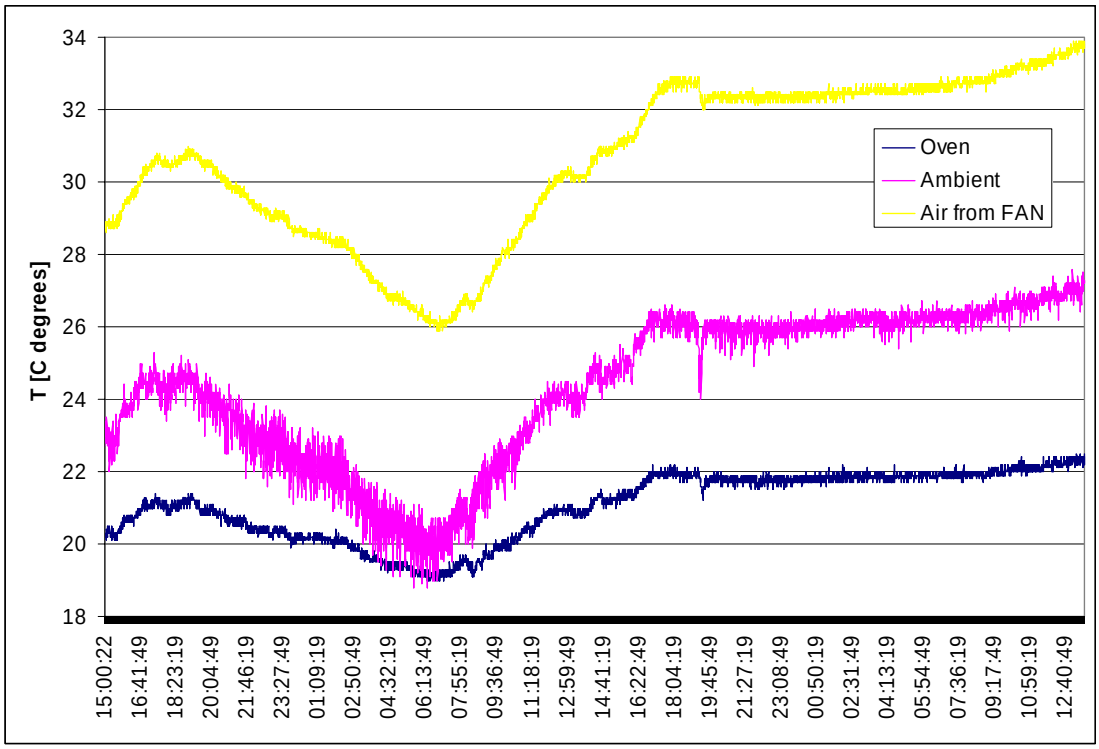

Figure 8.1.2: *Oven sensitivity to ambient temperature*

The oven temperature is following the ambient temperature but changes are suppressed:

Date	06:58:19	16:52:49	**ΔT [°C]**
T_ambient [°C]	19.9	26.2	6.3
T_oven [°C]	19.1	21.8	2.7

The oven temperature changes are $\frac{6.3}{2.7} = 2.3$ times less than the ambient temperature.

Conclusion:
Further temperature controller improvement is required.

Next step: I parameter is enabled to make it possible to increase the P gain.

8.1.3. Oven 1 temperature stability versus ambient with PI controller

Objective: Verifying of the oven performance after enabling I in the PI controller and increasing gain P

Procedure: The iDAQ was used to measure temperatures inside and outside of the oven.

Settings: The P gain was set to 90.
The I parameter was enabled. The integrator constant τ=3s.

Results:

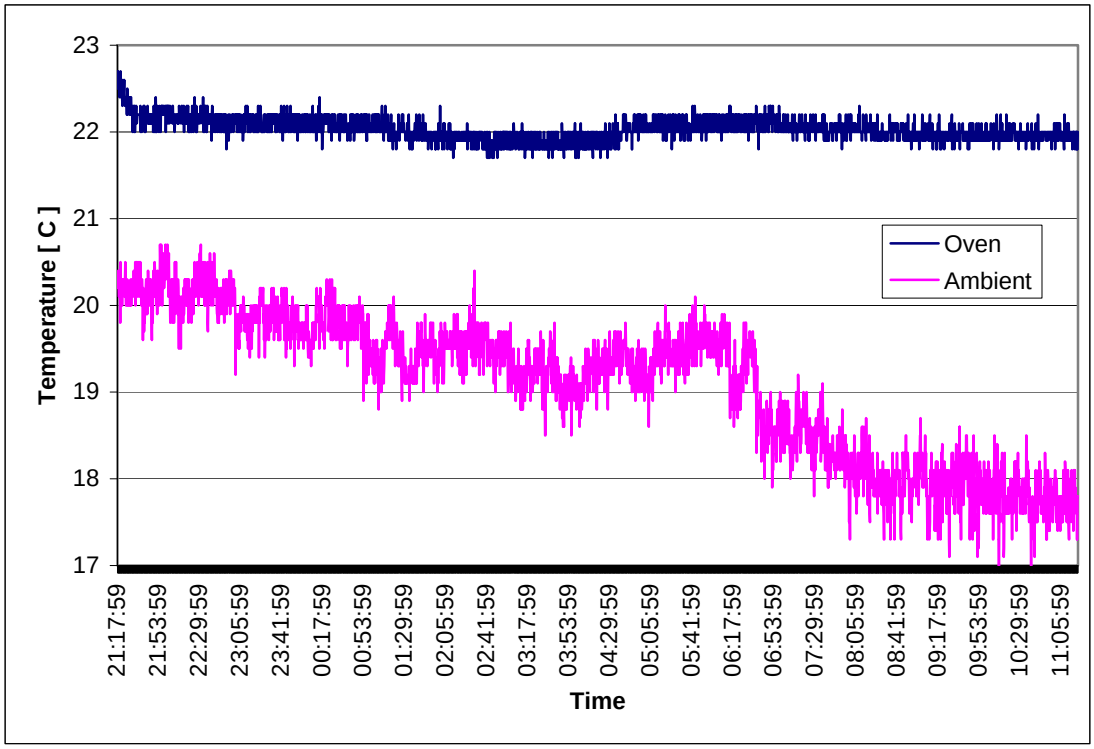

Figure 8.1.3: *Oven and ambient temperature vs. time.*

Observed ambient temperature change of ~2.8°C
Oven temperature change ~0.2°C

Conclusions: The goal has been achieved. Oven temperature remains relatively stable although the ambient temperature changes

Next step: Oven time response measurements.

8.1.4. Oven 1 time response overshoot measurements and optimization

Objective: Measurement of the temperature overshoot and finding the optimal values for P and I.
Procedure: The iDAQ was used to measure temperatures inside and outside of the oven.

The step response was measured for several different P gains with constant I=12s. In the previous measurement an overshoot was observed with I=3s. This could be minimized with decreasing the P gain but it would also affect the temperature stability. This is because with a low gain the oven controller cannot suppress the influence of ambient temperature changes. That's why the I parameter is increased instead of decreasing P in order to minimize the overshoot.

Settings: The P gain was set to 172 (R_{17}=38kΩ), 140 ((R_{17}=30.6kΩ) and 77 (R_{17}=17kΩ)

Results:

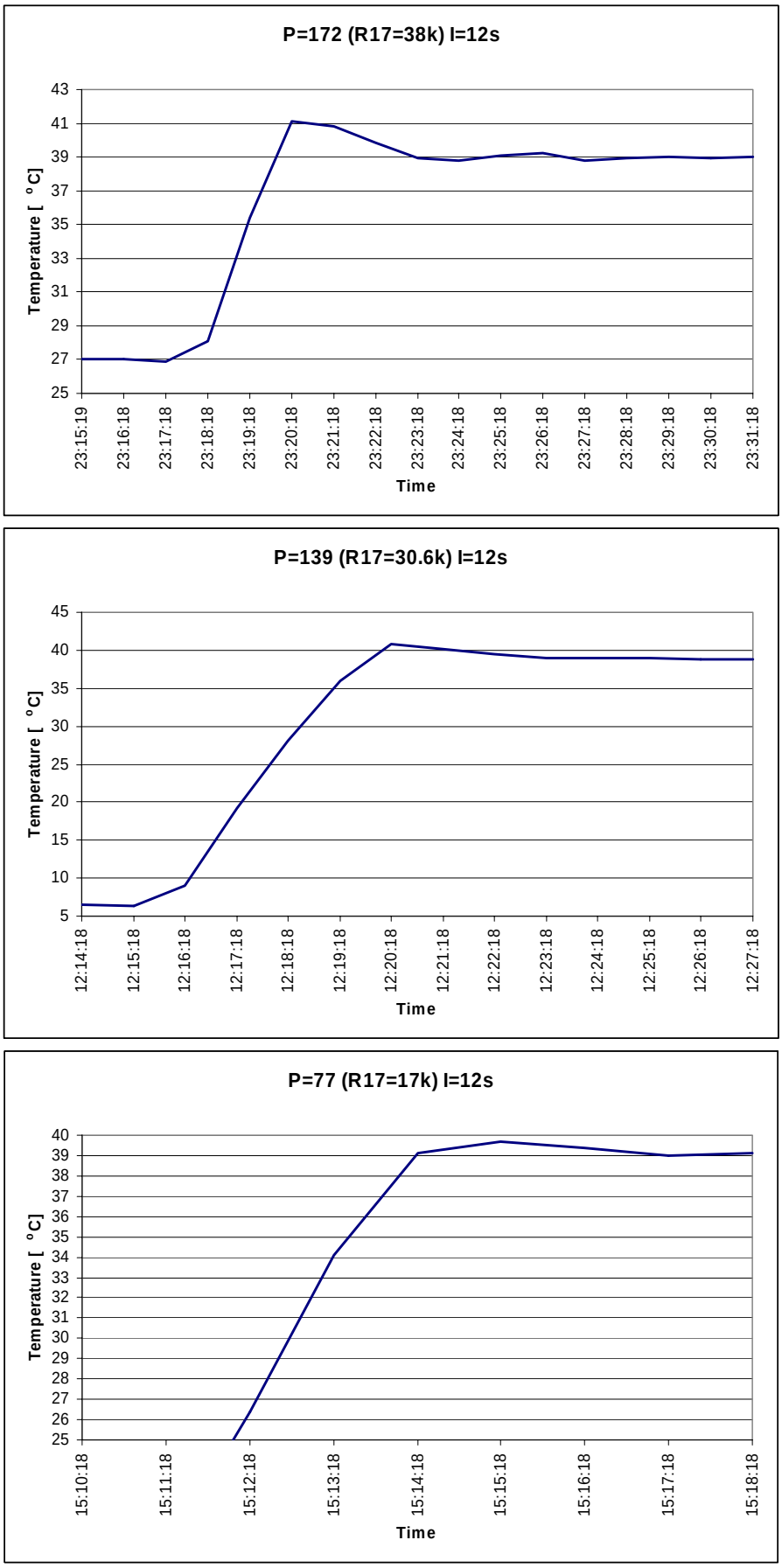

Figure 8.1.4: *Oven 1 temperature overshoot.*

Conclusions: following overshoot was observed:

P	Overshoot [^{o}C]
172	3
139	2
77	0.7

Probably for P<70 the overshoot could be removed. But further decrease in gain reduces temperature stability versus ambient temperature changes. The bigger the temperature step, the bigger is the overshoot. Here, it was measured for ΔT_{oven}>10^{o}C. In the feedback system, in steady state, the oven will probably operate with much smaller steps like few ^{o}C and so there will be no overshoot. It will be tested soon.

Assume that for further measurements the P is fixed to 90 (R_{17}=20kΩ).

Nest step: Measure the temperature stability over long time with ambient temperature changes.

8.1.5. Oven 1 temperature stability measurements with increased I parameter

Objective: Measurement of the oven temperature stability versus ambient temperature with P=90 and I=12s.

Procedure: The iDAQ was used to measure temperatures inside and outside of the oven.

Settings: P = 90 (R_{17} = 20kΩ).

Results:

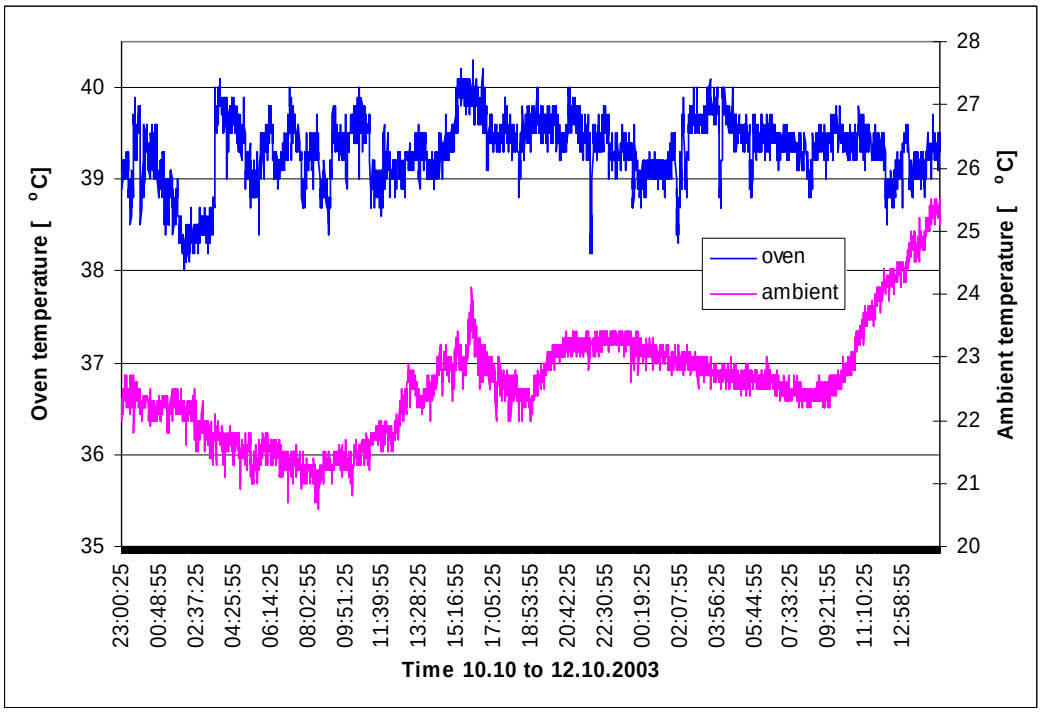

Figure 8.1.5: *Oven 1 temperature vs. time for increased integrator constant.*

Ambient temperature change of 5.5°C (p-p)

The oven temperature change is ~2°C (p-p) (10 times more than in preceding case- see 8.1.3) and it varied randomly independent of the ambient temperature. Several rapid jumps were observed.

Conclusions: The oven temperature gets unstable with increased integrator time constant. The reason may be the quality of the used capacitor (electrolyte) - the capacitance varies with time/temperature causing disturbances in the controller response. But we are not sure.

Next step: Decrease I or look for better capacitor.

8.1.6. Final oven 1 response measurements

Objective: Verifying of the temperature rise time and overshoot in the oven.

Procedure: The iDAQ was used to measure temperatures inside and outside of the oven. First, a large temperature step (20-37°C); next, a small step 20-25°C was measured

Settings: P = 90 (R_{17}=20kΩ) and I=3s. Good quality capacitors for the integrator used.

Results:

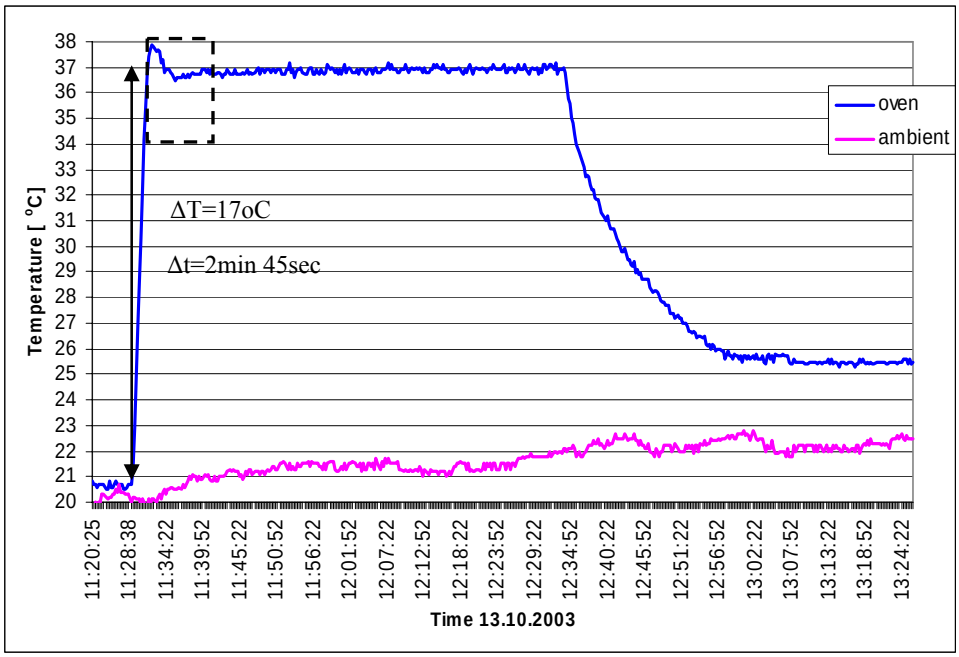

Figure 8.1.6: *Oven 1 step response.*

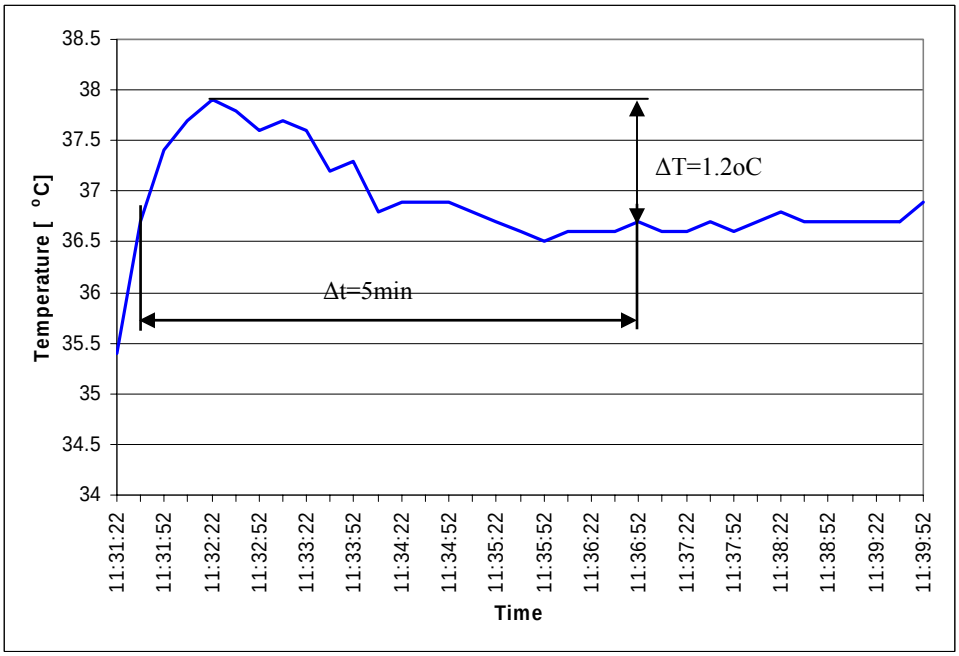

Figure 8.1.7: *Zoomed temperature rise top region from figure 8.1.6.*

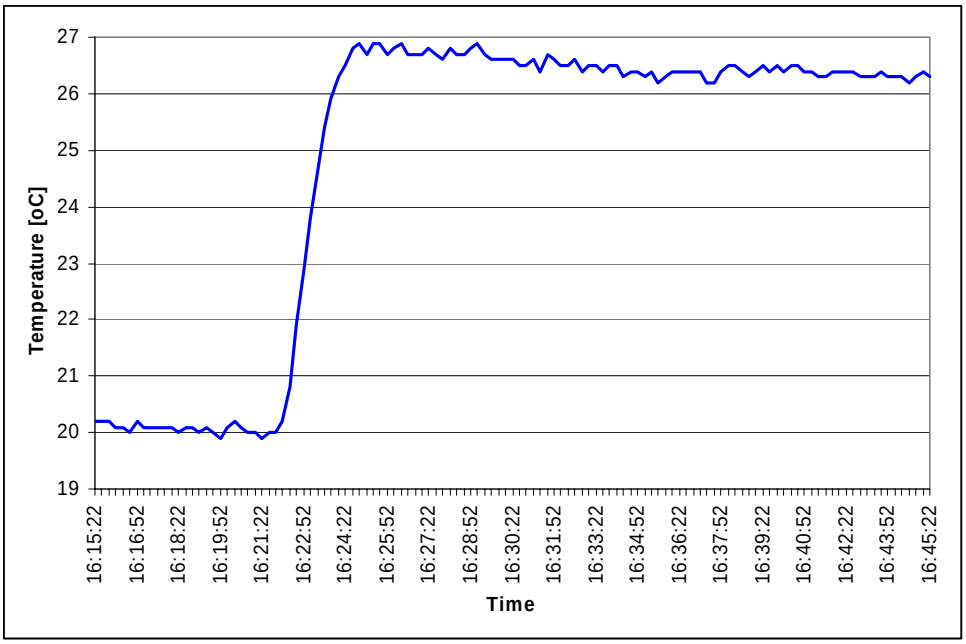

Figure 8.1.8: *Oven temperature rise for step 20°C to 27°C.*

Conclusions: Overshoot of 1.2°C after temperature step 20-37°C (see fig. 8.1.7) and 0.5°C after step 20-27°C (see fig. 8.1.8). Smaller steps are expected when feedback system is working, so the oven performance may be satisfying.

The change of the temperature from 20 to 37°C takes about 7 min and 45 sec but the last 5 minutes are needed for stabilizing the 1.2°C overshoot. Such performance is satisfying for use in the feedback scheme.

Over a long time the temperature follows slightly the ambient temperature but it remains within the 0.2°C range when ambient changes ~2.5°C.

Next step: Long term temperature stability must be tested.

8.1.7. Final oven 1 temperature stability measurement

Objective: Verifying of the oven temperature stability versus ambient temperature with P=90 and I = 3s.

Procedure: The iDAQ was used to measure temperatures inside and outside of the oven.
Results:

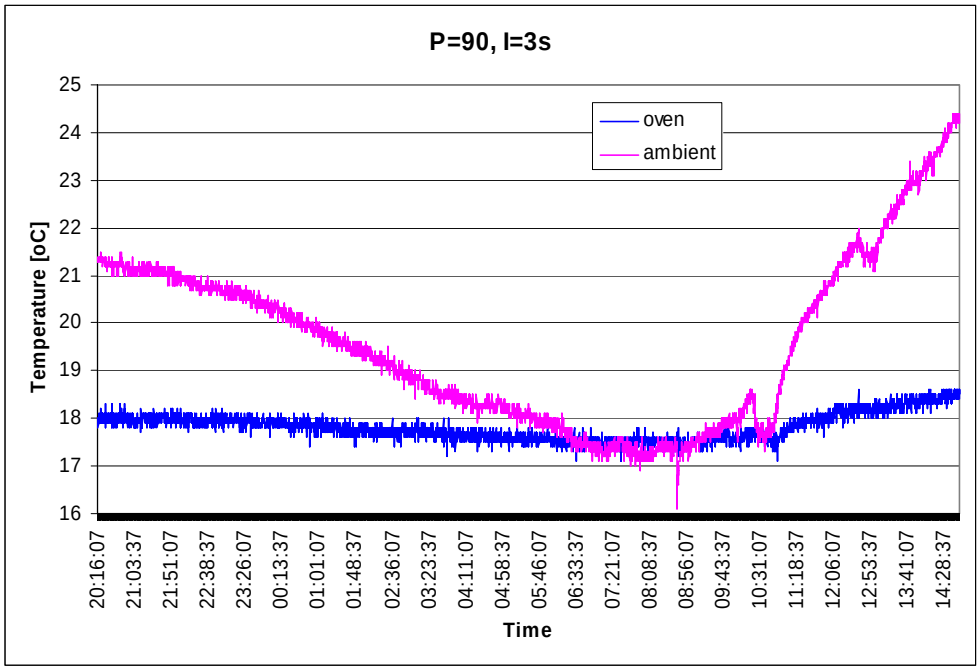

Figure 8.1.9: *Oven 1 temperature vs. time.*

Observed temperature drift:

	min	max	ΔT
T. Oven [^{o}C]	17.5	18.6	1.1
T. Ambient [^{o}C]	17.3	24.4	7.1

So the oven temperature changes as 1.1/7.1=0.15 ^{o}C/ambient ^{o}C
Such changes can be corrected by the feedback loop of the FO system controller. There is no further need for optimization.

8.2. OVEN2 PERFORMANCE TESTS

This chapter describes measurement of parameters of the oven designed for the optical phase shifter purpose – as described in chapter 6.2. Tests of oven 2 similar to oven 1 tests were made. There were several iterations of measurements before proper values for PI controller parameters were found. Figures 8.2.1 and 8.2.2 show results of the final oven 2 measurements. The oven temperature remains stable (<<0.5^{o}C p-p) vs. time if no set-point

changes are made. But the ambient temperature was also stable. Oven temperature stability test against ambient temperature is planned with the use of the climate chamber.

Zoom of the plot in figure 8.2.2 shows about 5 minutes rise time for +10°C temperature step and ~ 18 minutes fall time for -20°C temperature step. Slower cooling than heating is caused by TEC element features – the heat-flow differs in both directions.

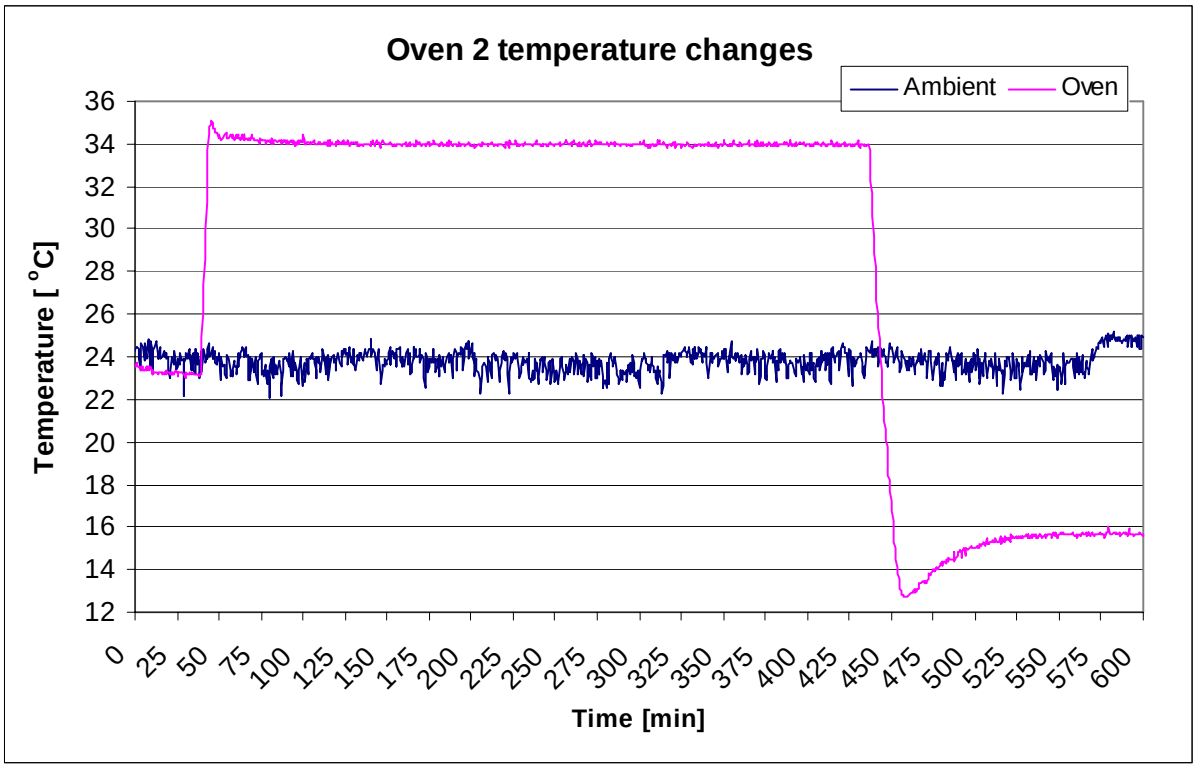

Figure 8.2.1: *Final oven 2 performance measurements.*

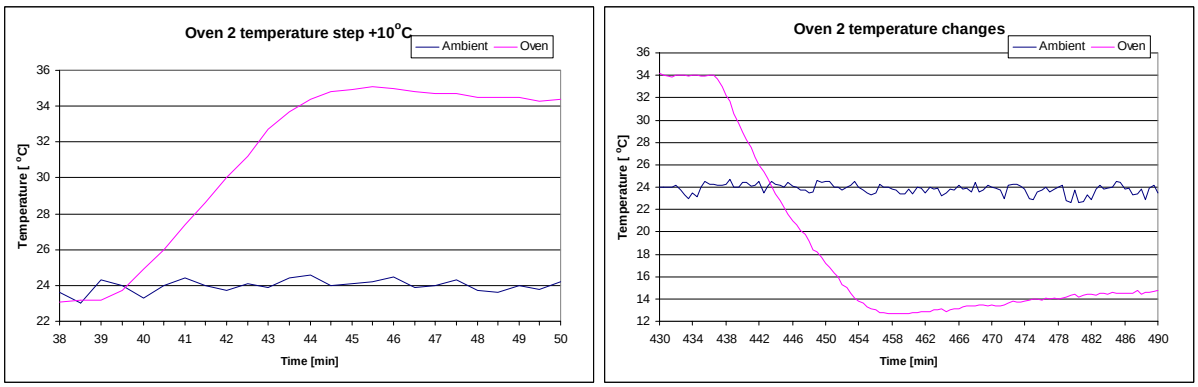

Figure 8.2.2: *Zoomed regions of oven 2 temperature rise and drop from figure 8.2.1.*

8.3. PHASE DETECTOR

The HMC403 digital phase detector (P.D.) circuit as described in section 6.4 is tested. The phase detector is one of the most critical components in the FO system when the output signal phase stability is considered. Therefore much effort is put in evaluating the P.D. performance. First measurements were done with home-made Printed Circuit Board (PCB) called further "old detector" and later a professional PCB was manufactured, which will be called further "new detector". In some cases differences in the behavior of both devices can be observed.

The measurement of the full scale range of the P.D. voltage and gain (in mV/^{o}) is performed. Desired is 3.6 V full scale range with the gain of 10mV/^{o}. Later the P.D. sensitivity to ambient temperature changes is tested and approximate linearity test is performed.

8.3.1. Output full scale range

The measurement setup is shown in figure 8.3.1. The oven and spool with fiber was used to generate a phase change of one of the signals. The entire measurement setup was installed inside the climate chamber and it was temperature stabilized at 21^{o}C to prevent errors from ambient temperature changes. An additional measurement was performed where phase change was generated using two unlocked oscillators – the obtained results are similar and not presented here.

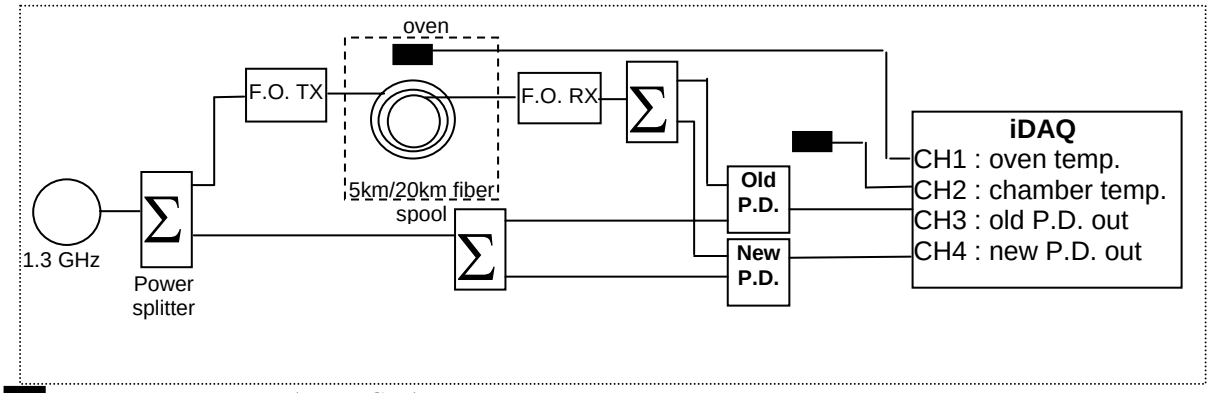

Figure 8.3.1: *P.D. full range and gain measurement setup*

Measurement procedure:

1. Cool down fiber spool to 15ºC, wait for stable conditions.
2. Make temperature step on fiber to about 30ºC, wait for stable conditions.
3. Cool down again to 15ºC, wait for stable conditions.

Example measurement results are shown in figure 8.3.2. Observed is a saw-tooth like curve.This is because the input signal phase change exceeds the P.D. input range. By substracting the minimum and maximum values one gets the full scale voltage range. The P.D. gain is found by dividing full scale range by 360^{o}.

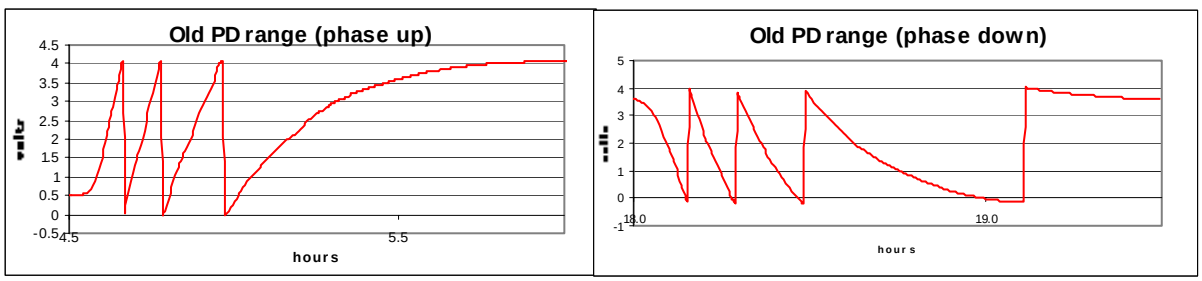

Figure 8.3.2: *Example of P.D. output voltage.*

Table 8.3.1: *Phase detector full range and gain.*

	Output range [V]	P.D. gain [mV/ o]
Old detector	**74.2**	**11.7**
New detector	**4.1**	**11.3**

Summary of the measurement results is given in table 8.3.1. Performed measurements show that the gain and the output range of the detectors are not significantly temperature dependant. It is also observed, that the faster the phase change is, the higher the full range and gain. It is easy to observe with mentioned above two oscillator measurement method. Of course at some speed of phase change (high sawtooth-oscillation frequency at P.D. output) the output range is decreased because of low-pass filtering in the P.D. The gain change was not large ~5% max. The explanation of gain decrease for slow input signal phase changes is unknown.

8.3.2. Phase detector sensitivity to temperature

The phase detector temperature sensitivity was tested by heating and cooling the P.D. while a constant phase difference of the input signals was maintained – see figure 8.3.3. Two detectors were tested in parallel.

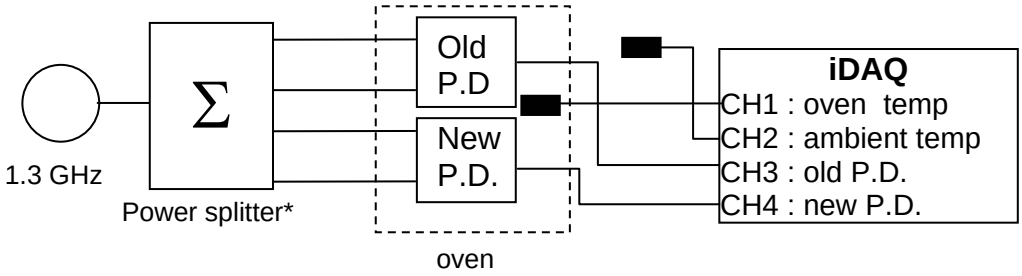

Climate Chamber – 21ºC

*) To be exact three two-way power splitters were used here.

Figure 8.3.3: *Phase detector sensitivity to temperature test*

Measurement procedure:

1. Cool down detectors to 15ºC, wait for stable conditions.
2. Heat phase detectors to about 30ºC, wait for stable conditions.
3. Cool down again to 15ºC, wait for stable conditions.

Measurement results are shown in table 8.3.2 and figure 8.3.4. The start and end temperature levels differ during the temperature steps down and up. The measurement data was taken at different times with a bit different settings but this doesn't influence the result accuracy. One can clearly see that the new P.D. response is correlated with temperature. The old P.D. board behaves different. This is difficult to explain because both circuits are almost the same. The RF cable sensitivity to temperature can be excluded because both input cables inside the oven are of the same type and length so temperature changes affect both input signals the same way and should not influence P.D. input phase difference.

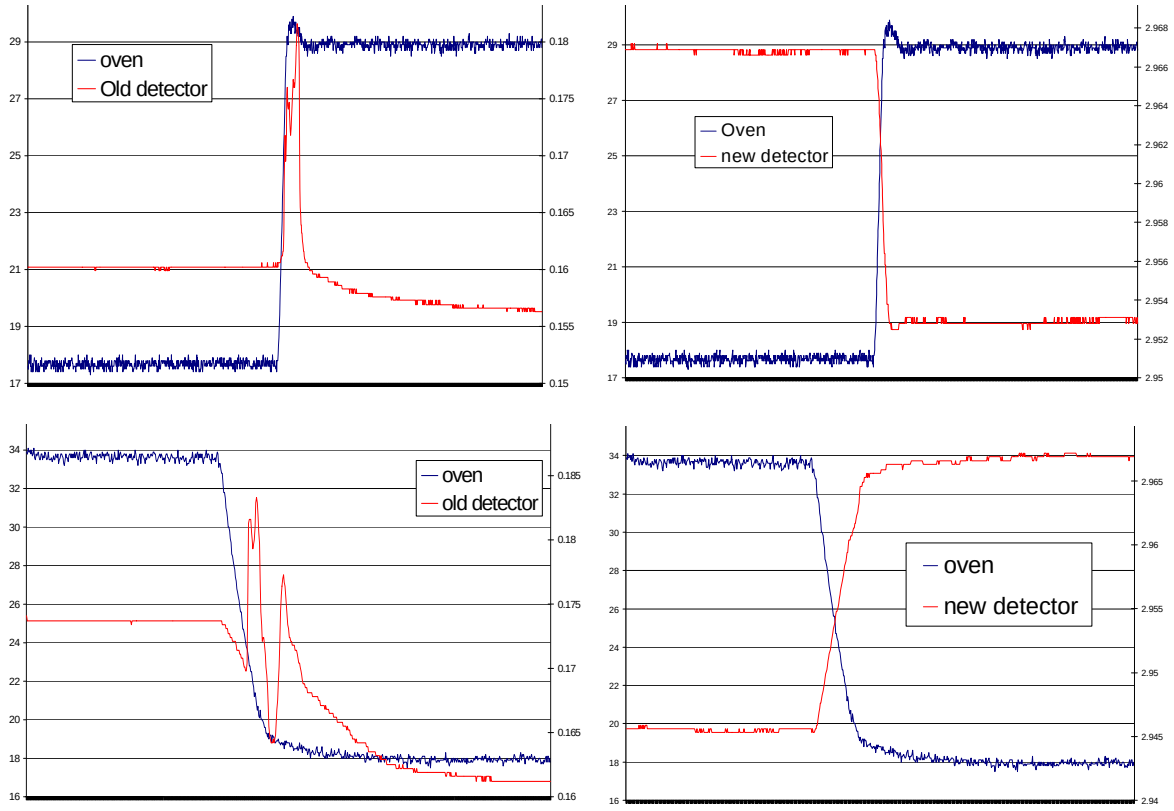

Figure 8.3.4: *Phase detector sensitivity to temperature.*

Table 8.3.2: *Phase detector sensitivity to temperature values.*

		Old detector			New detector		
	ΔT [ºC]	ΔU [V]	Δφ [º]	Δφ/ΔT [º/ºC]	ΔU [V]	Δφ [º]	Δφ/ΔT [º/ºC]
17.7ºC → 28.9ºC	11.2	-0.004	-0.34	**-0.031**	-0.014	-1.24	**-0.111**
33.7ºC → 17.9ºC	-15.8	-0.013	-1.11	**0.070**	0.021	1.86	**-0.118**

From this measurement it is impossible to precisely predict old P.D. behavior because it could have either positive or negative temperature coefficient.

Conclusion

1. The new detector board has a negative temperature coefficient
2. The old detector shows "strange" behavior
3. The temperature sensitivity is on an acceptable level for the FO system - ~0.1°/°C if no larger ambient temperature variations than 1°C are assured. For this care must be taken of temperature stabilization of phase detectors.

8.3.3. Hysteresis

For evaluating the P.D. performance as shown in figure 8.3.5 – a mechanical phase shifter was used with about 15 cm electrical path length adjustment range – see figure 8.3.6. The P.D. output voltage was measured while changing phase shifter setting – it has a precise (1μm resolution) scale.

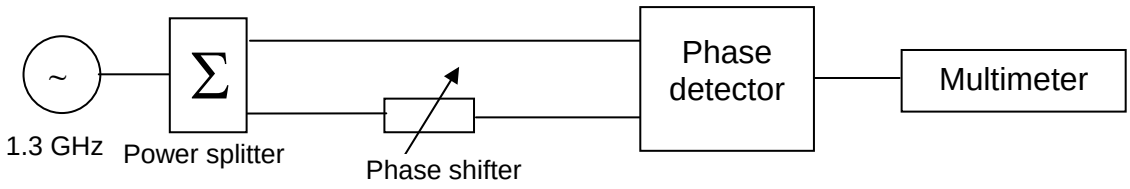

Figure 8.3.5: *Phase shifter measurement.*

Figure 8.3.6: *Mechanical phase shifter.*

Measurement results are shown in figure 8.3.7. A hysteresis is observed on the plot. Most probably it comes from the mechanical properties of the phase shifter and it is not a P.D. feature but those results are attached here because during this test it was noticed that, especially the new P.D. characteristic has clear nonlinearities. Those nonlinearities were investigated later and are described it in the next section.

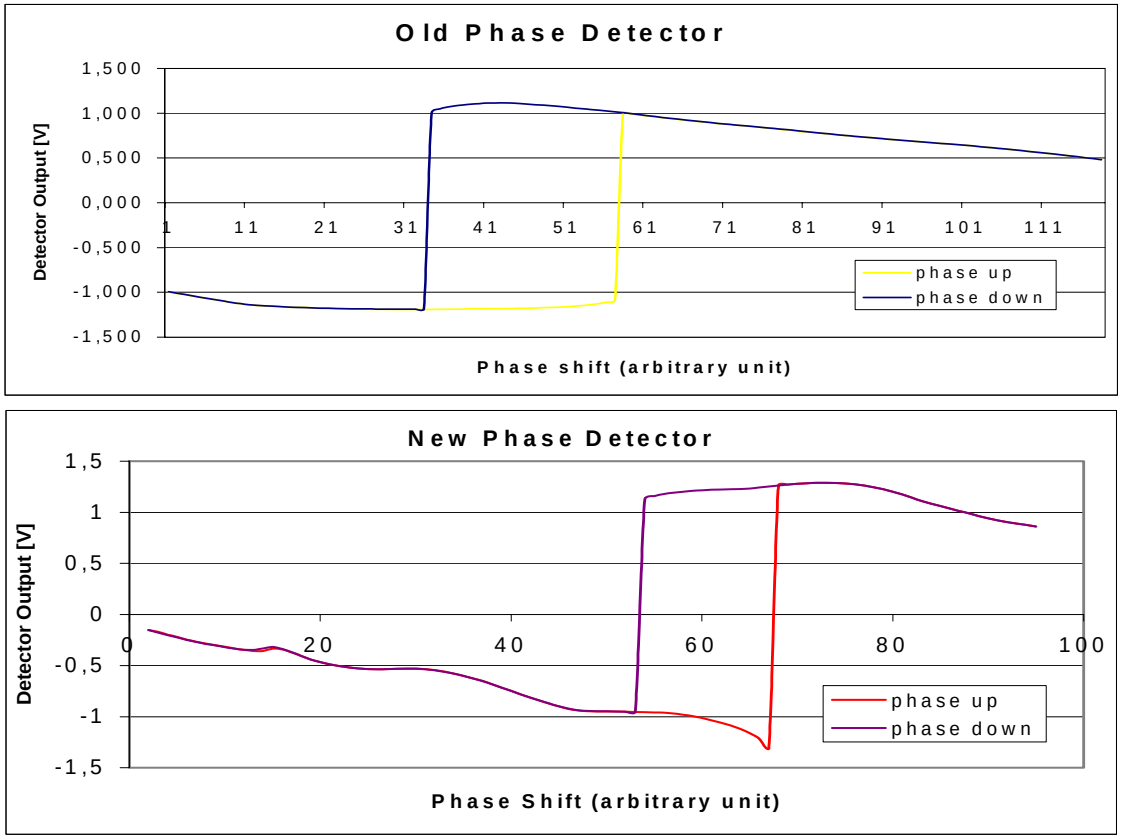

Figure 8.3.7: *Hysteresis measurement results.*

Note: This measurement was done in the office so there may be a significant error due to ambient temperature changes.

Short hysteresis measurement summary:

Old Detector: Hysteresis is about 240 units of the phase shifter
Assumptions: - signal wavelength $\lambda = 0.23$m,
- unit of the phase shifter is 1 μm => 240μm
→ Hysteresis ≈ (0.00024m/0.23m)*360º ≈ **0.37º**

New Detector: Hysteresis is about 280 units of the phase shifter
Same assumptions as for old detector
→ Hysteresis ≈ (0.00028m/0.23m)*360º ≈ **0.43º**

These values are small but it must be remembered in some cases when using this mechanical phase shifter!

8.3.4. Phase detector nonlinearities

As mentioned in the preceding section the phase detector characteristic shows significant nonlinearities. Therefore, the data measured for section 8.3.1 - see figure 8.3.2 - is investigated more precisely. Figure 8.3.8 shows zoomed plots of the output signals of both phase detectors scaled in degrees. A significant nonlinearity of the new detector is clearly to be observed. The curve of the old P.D. is also nonlinear but not so much. Nonlinearities most probably result from the internal structure of the HMC403 device.

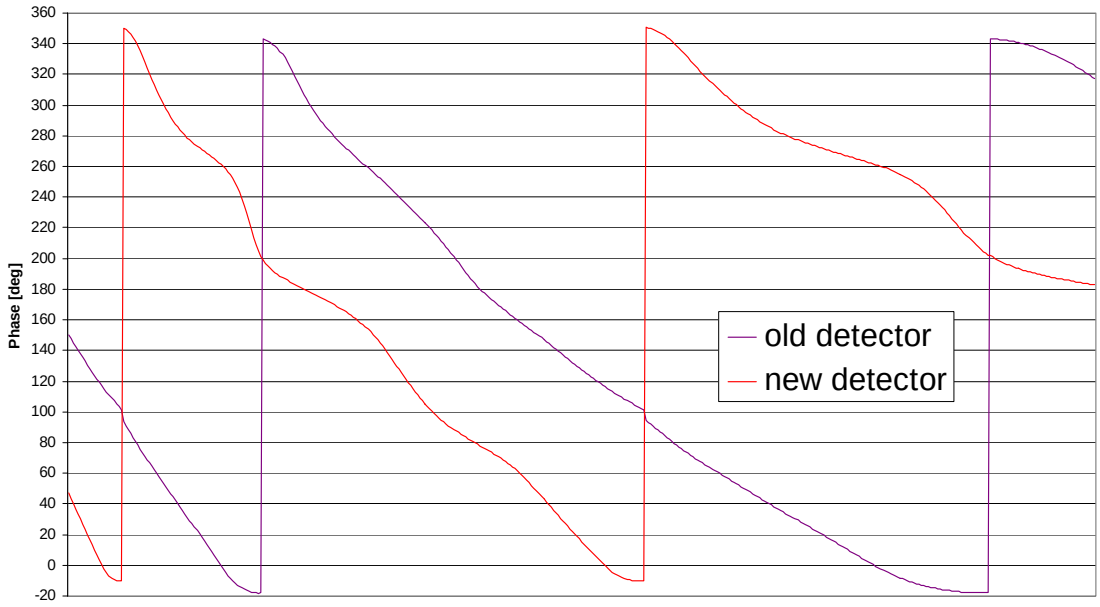

Figure 8.3.8: *Phase detector nonlinearities.*

This measurement can not be considered as precise because the spool with fiber placed inside the oven was used to generate phase changes. The velocity of phase change in time may vary because of non constant heating speed of the oven. So the x-axis scale is not defined in this case and differences from expected ideal characteristic can not be calculated using this

data. More precise measurements of the nonlinearity using another measurement setup is planned in near future.

8.4. LASER TRANSMITTER

8.4.1. Temperature Sensitivity

Measurement of the laser transmitter (described in section 6.3) sensitivity to temperature is made - see figure 8.4.1 for block diagram. The laser temperature was changed and the output signal phase change was measured while keeping the entire system temperature constant (+21°C) inside of the climate chamber.

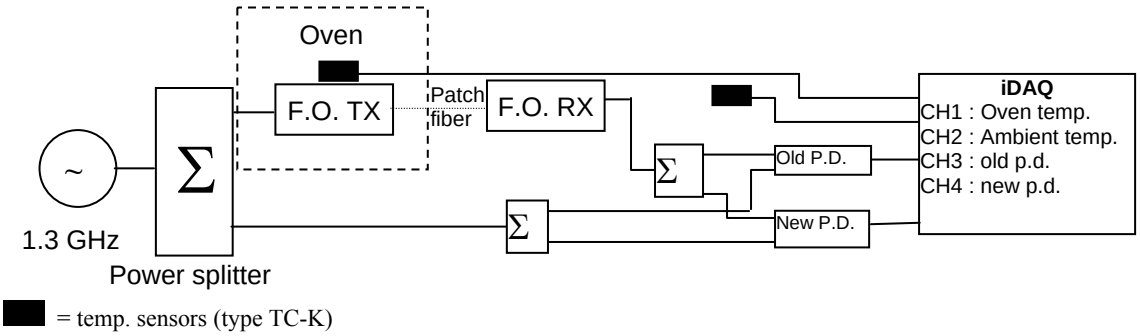

Figure 8.4.1: *Measurement of laser transmitter sensitivity to temperature.*

Results of the measurements are shown in figure 8.4.2 and table 8.4.1. On the data plot it can be seen that phase changes are correlated to temperature changes but in the left part of the plot (before the temperature step) the phase rises while the temperature remains relatively constant. Most probably the temperature step was applied to early – in self heating stage of the laser transmitter.

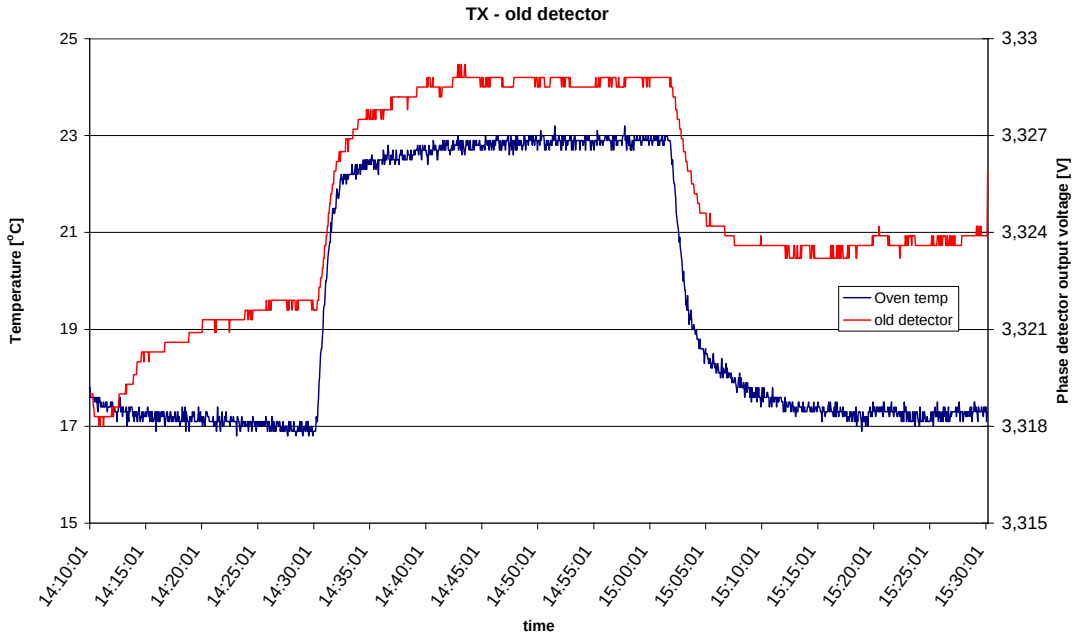

Figure 8.4.2: *Laser transmitter temperature sensitivity measurement.*

Results summarized in table 8.4.1 show that the laser sensitivity to temperature does not exceed $0.1^{o}/^{o}C$. It means that larger temperature changes for the laser module should be prevented while operating the FO system.

Table 8.4.1: *Summary of the laser transmitter temperature sensitivity measurements*

Temperature step	ΔT [ºC]	ΔU [mV]	Δφ [º]	Δφ/ΔT [º/ºC]
16.9ºC – 22.9ºC	6	7 (old det)	0.6	**0.1**
		4 (new det)	0.4	**~0.06**
22.9ºC – 17.3ºC	5.6	6 (old det)	0.5	**~0.09**
		5 (new det)	0.4	**~0.07**

8.5. FIBER-OPTIC RECEIVER

Two receiver modules manufactured by Spinner (see section 6.5) were used.
Receiver one (RX1) serial number is S03276
Receiver two (RX2) serial number is S03275

Temperature sensitivity measurement has been performed the same way as for the laser transmitter. The Receiver temperature was changed in the oven and the phase change of the signal was measured while all system components were temperature stabilized inside the climate chamber – see figure 8.5.1.

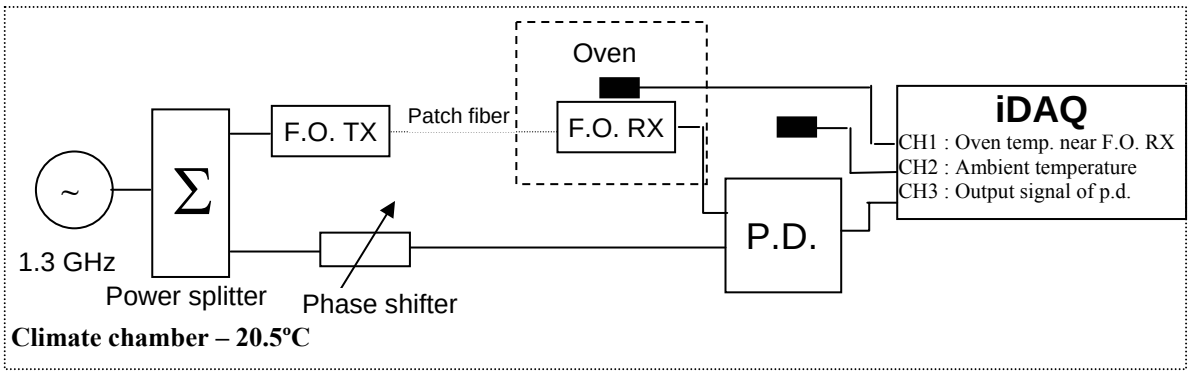

Figure 8.5.1: *Measurement of fiber optic receiver sensitivity to temperature*

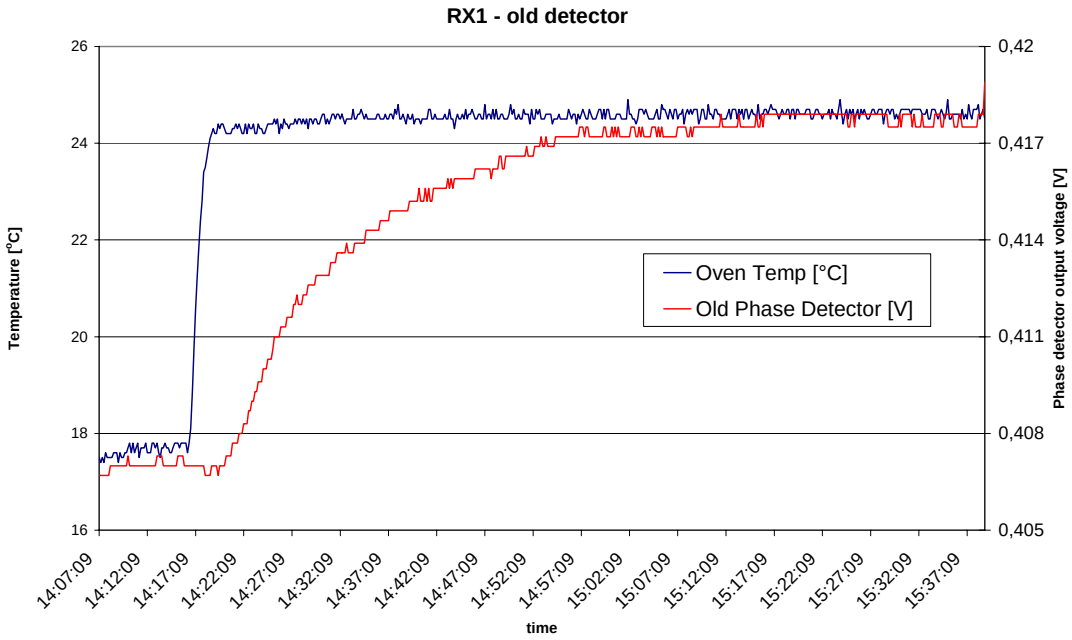

Figure 8.5.2 *Measurement results of the fiber optic receiver temperature sensitivity.*

An example of the measurement results of the receiver 1 is shown in the figure 8.5.2. All results are summarized in the table 8.5.1. The phase sensitivity to temperature is below $0.1^{o}/^{o}C$ and 0.05 $^{o}/\ ^{o}C$ at the measurement, made with the new phase detector. It looks like there is a significant measurement error but it can be assumed that the receiver sensitivity is smaller than $0.1^{o}/^{o}C$.

Table 8.5.1: *Summary of the fiber optic receiver temperature sensitivity measurements*

	ΔT [ºC]	ΔU [mV]	Δφ [º]	Δφ/ΔT [º/ºC]
RX1	*6.7*	*9.5 (old det.)*	*8*	***1.20***
	6.9	11.0 (old det)	0.9	**0.10**
	6.9	4.0 (new det)	0.4	**0.05**
RX2	8.8	10.0 (old det)	0.9	**0.10**
	8.8	4.0 (new det)	0.4	**0.04**

Similarly to the laser transmitter the sensitivity to temperature is relatively small but larger temperature changes for the FO-Rx module should be prevented while operating the FO system.

8.6. OPTICAL TRANSFER LINE

When connecting laser transmitter (FO-Tx) and fiber optic receiver (FO-Rx) with optical fiber an analogue optical transfer line is obtained. In this section tests of this line are described. The 3 dB bandwidth measurements are presented. Planned are measurements of the 1 dB compression point value and the RF gain of the link.

The 3dB bandwidth

The magnitude of the signal going through the link vs. frequency was measured using a network analyzer. The device was calibrated previously but there is no certainty about the accuracy of this calibration and unfortunately a calibration kit was not available. So, the

obtained measured magnitude values should be considered as qualitative only, but not as a precise result. Fortunately the calibration shouldn't affect significantly the 3dB bandwidth measurement because the 3dB curve drop is searched relating to the maximum value.

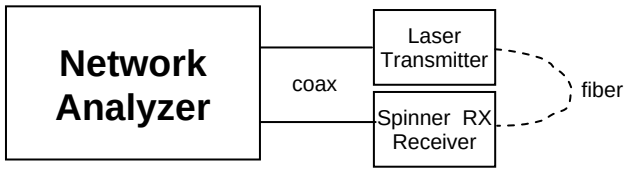

Figure 8.6.1: *The 3dB bandwidth measurement of the optical link.*

Measurement setup is shown in figure 8.6.1 and results in figure 8.6.2.

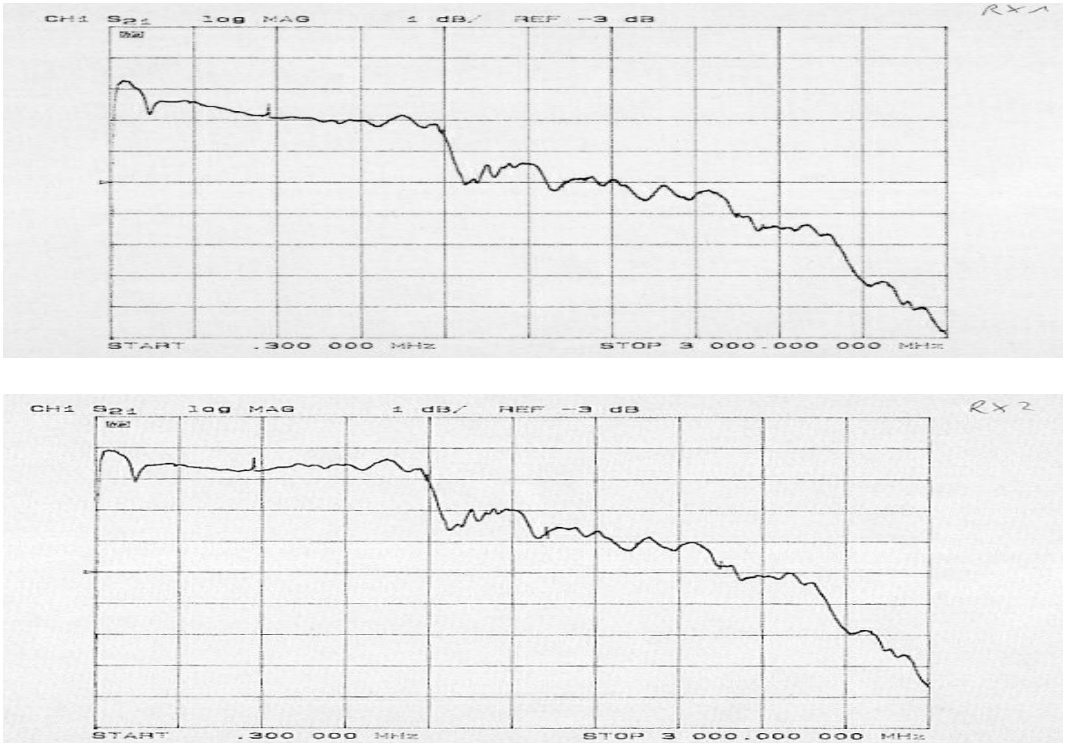

Figure 8.6.2: *3dB bandwidth measurements of FO link; upper plot – with Rx1, plot below – with Rx2*

Table 8.6.1: *Summary of the FO link 3dB bandwidth measurements*

	RX1	**RX2**
Maximum	50MHz, +0.55dB	50MHz, +0.9dB
Max – 3dB (lower frq)	11MHz	10MHz
Max – 3dB (upper frq)	1.25GHz	1.87GHz
9MHz	-4.5dB	-3.3dB
81MHz	+0.25dB	+0.8dB
1.3GHz	-3dB	-1.5dB
2.856Ghz	-6.7dB	-5.5dB

The 3 dB bandwidth of the link with Rx1 is small - 1.25 GHz. This is difficult to explain with the measured data. The measurement will be repeated because the expected bandwidth is about 2 GHz.

8.7. SPOOL WITH 5km OF OPTICAL FIBER

8.7.1. Temperature sensitivity

The sensitivity of the signal in the fiber to temperature changes was measured in order to verify data given by the fiber manufacturer. The fiber phase length vs. temperature coefficient value was given 10ppm/^{o}C. The oven was used to change the temperature of the fiber (see figure 8.7.1). Several measurements were made with old and new detector and also the phase change when temperature was rising and falling was measured. A precise oven temperature control was not ready in the time of making this measurement therefore temperature step values differ for different measurements. But it doesn't affect results.

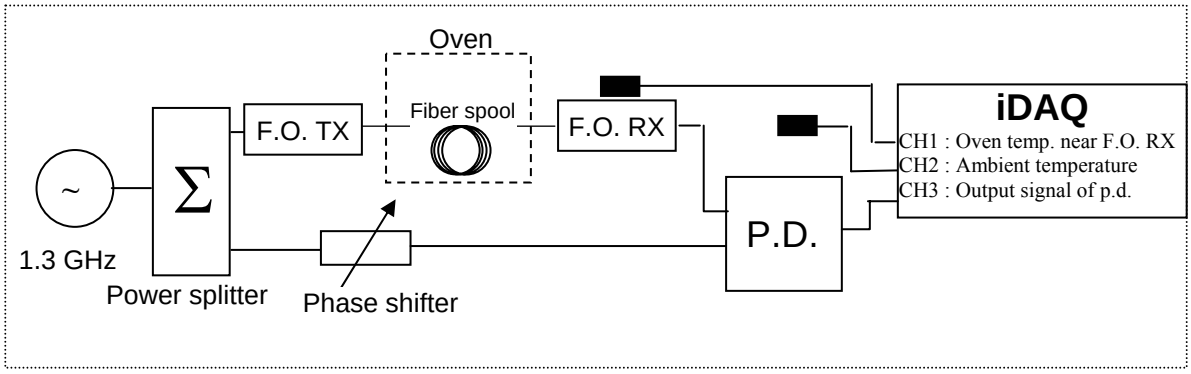

Figure 8.7.1: *Fiber sensitivity to temperature measurement.*

Provided temperature changes on 5 km long fiber were about 15^{o}C. Corresponding phase change exceeded significantly 360^{o} – range of the phase detector. Therefore the obtained plot was saw-tooth like (see figure 8.3.2). Measured data after unwrapping is shown in figure 8.7.2 and 8.7.3. The summary of all performed measurements is given in table 8.7.1.

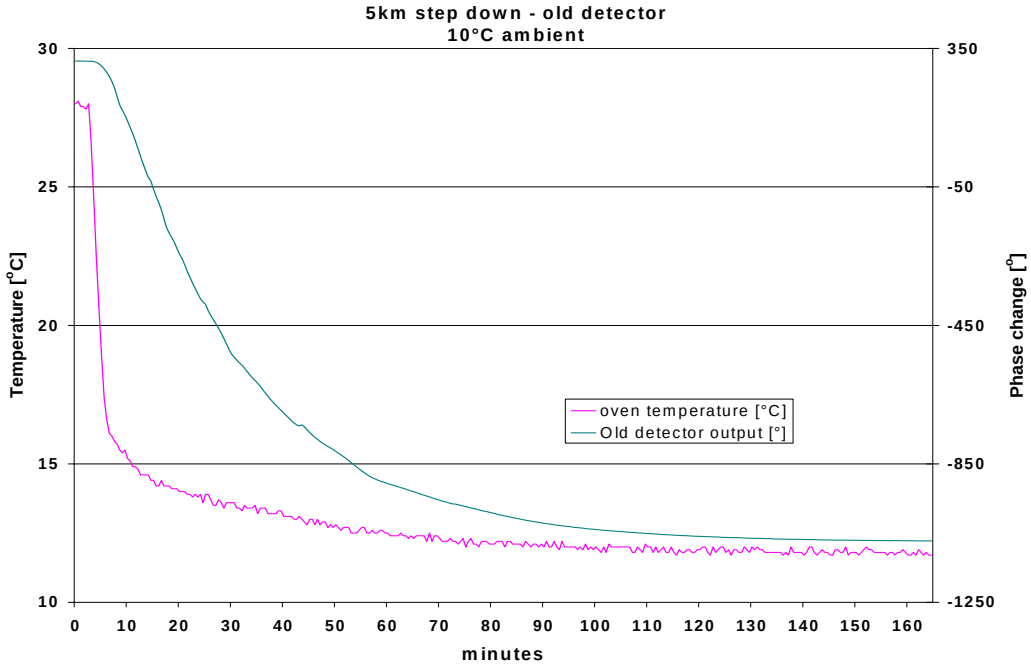

Figure 8.7.2: *Signal phase change in fiber when negative temperature step provided.*

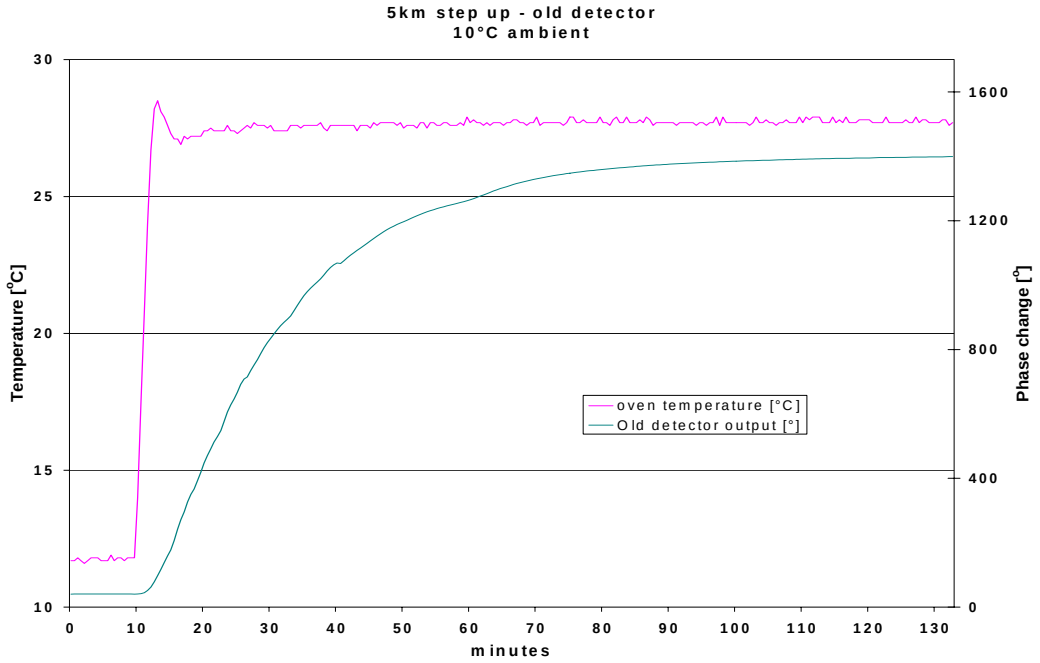

Figure 8.7.3: *Signal phase change in fiber when positive temperature step provided.*

For having a good view on the results the obtained phase change values are given in degree and in ps unit (Δφ [ps] column in the table). The temperature sensitivity of the spool was calculated in degrees and picosecond per ^{o}C units. There are small differences in results from different measurements, but only in single percent range and were caused by measurement method inaccuracy. Interesting is that the measured phase length vs. temperature coefficient is smaller (~7.5 ppm/^{o}C) than given in the fiber datasheet provided by manufacturer (10 ppm/^{o}C). But of course it is better for the application in reference frequency distribution system because it means that there will be necessity of correcting smaller errors in the long link.

Important observation from this measurement that must be noticed is the range of phase change which exceeds 1300^{o}! Of course in the accelerator tunnel there will rather be smaller temperature changes than 15^{o}C but for the TESLA project link length may exceed 15 km and even if temperature changes of single C degrees, there will be hundreds of degrees of signal phase change!

Table 8.7.1: *Fiber spool temperature sensitivity measurement summary*

		ΔU [V]	Δφ		ΔT [^{o}C]	Δφ/ΔT		Tk_{phase} [ppm/ $_{o}$C]
			[^{o}]	[ps]		[^{o}/ ^{o}C]	[ps/ ^{o}C]	
Old phase detector	Phase shift up	15.9	1359	2904	16.0	84.9	181.5	7.4
		16.1	1380	2949	16.5	83.6	178.7	7.3
		14.9	1270	2714	14.9	85.2	182.1	7.4
	Phase down	16.2	1386	2962	16.2	85.6	182.8	7.5
		16.8	1440	3077	16.8	85.7	183.1	7.5
		13.8	1181	2524	12.9	91.6	195.6	8.0
New detector	Phase up	15.3	1354	2893	16.0	84.6	180.8	7.4
		14.2	1258	2688	14.9	84.4	180.4	7.4
	Phase down	15.6	1377	2942	15.6	88.3	188.6	7.7
		13.3	1179	2519	13.3	88.6	189.4	7.7

Equations are given below that were used to calculate data collected in table 8.7.1.

The conversion from [°/°C] to [ps/°C] is:

$$\left[\frac{ps}{^\circ C}\right]=\left[\frac{^0}{^\circ C}\right]*\left[\frac{ps}{^0}\right] \quad x=\frac{\Delta\varphi}{\Delta T}*\frac{T}{360^0}$$

T: 1/f period time (T=769ps)
x: Phase change per °C in ps
ΔT: Temperature step in ºC

Time, the signal needs to pass 5 km of fiber: $t=\frac{1}{c_0}*n=\frac{5000m}{3*10^8 m/s}*1.4682=24.5\mu s$

l: length of line,
n: refraction index
c_0: speed of light in vacuum

The phase length vs. temperature coefficient value:

$$ppm=\frac{x}{t}*10^6$$

$$\rightarrow\left[\frac{ppm}{K}\right]=\frac{\Delta\varphi}{\Delta T}\left[\frac{^\circ}{^\circ C}\right]*0.08732\left[\frac{1}{^\circ}\right]$$

8.7.2. Time constant / rise time

To calculate the FO system PID controller parameters it is necessary to find the response of the spool with fiber on the temperature step. Here the time response depends also on the oven properties because the spool was tested by providing temperature step inside the oven. The speed of temperature changes inside the oven is of course limited see sections 8.1 and 8.2. The test-system setup was same as for temperature sensitivity measurement (section 8.7.1 and figure 8.7.1) but during this measurement the time of signal phase changes in the fiber was analyzed.

The summary of measurements of 5 km spool time responses is given in tables 8.7.2 and 8.7.3. Phase changes were measured with old and new phase detector board connected in parallel. Measurements were performed at several ambient temperatures (controlled by climate chamber) because oven response depends on the ambient temperature. The total spool temperature change inside the oven (ΔT) was given and also given was measured range of phase detector output voltage ΔU, converted to degrees of phase change (Δφ).

Table 8.7.2: *Fiber spool time constant measurement summary for rising temperature value*

	Amb T [°C]	ΔT [°C]	ΔU [V]	Δφ [°]	τ [s] 0-63% time constant	Δt [s] 10-90% rise time	t_d [s] 0-10% delay time	t_t [min] 0-100% total time
Old phase detector	10	16.0 (12 - 28)	15.9	1359	1380 (23min)	2700 (45min)	330 (5.5)	122
	20	16.5 (14 –30.5)	16.1	1380	1500 (25min)	2190 (36.5min)	558 (≈9min)	90
	30	14.9 (17 –31.9)	14.9	1270	1530 (25.5min)	3180 (53min)	300 (≈5min)	125
New detector	10	16.0 (12 - 28)	15.3	1354	1860 (21.5min)	2360 (≈39min)	300 (5min)	122
	30	14.9 (17 – 1.9)	14.2	1258	1530 (25.5min)	3000 (50min)	330 (≈5.5min)	125

Table 8.7.3: *Fiber spool time constant measurement summary for decreasing temperature value*

	Amb T [°C]	ΔT [°C]	ΔU [V]	Δφ [°]	. τ [s] 0-63% time constant	Δt [s] 10-90% rise time	t_d [s] 0-10% delay time	t_t [min] 0-100% total time
Old phase detector	10	16.2 (28 – 11.8)	16.2	1386	1920 (32min)	3420 (57min)	510 (8.5min)	165
	20	16.8 (31 – 4.2)	16.8	1440	1440 (24min)	2370 (39.5min)	3600 (6min)	115
	30	12.9 (30 -17.1)	13.8	1181	1470 (24.5min)	2600 (43.3min)	3600 (6min)	125
New detector	10	16.2 (28 -11.8)	15.6	1377	1950 (32.5min)	3420 (57min)	564 (9.4min)	165
	30	12.9 (30 – 7.1)	13.3	1179	1450 (24.2min)	2460 (41min)	3610 (6.2min)	125

Observed was a time constant of 20 to 25 minutes, a rise- and fall-time of 45±10 minutes and a delay time of 5 to 9 minutes. The delay time was defined as the time when phase change reaches 10% of maximum value. The time needed to be able to detect phase change after providing temperature step is much shorter – 6 – 8 seconds. Oven temperature starts changing after 3- 4 second.

9. SYSTEM ASSEMBLY AND PERFORMANCE TESTS

9.1. SYSTEM SETUP

After building and gathering all system components test setup for the FO system prototype was prepared. Block diagram of the system test setup is shown in figure 9.1.1. The only difference from the destination FO system (see figure 3.1) is that here a long link simulator was used which was made of an oven and a spool with 20 km of fiber. The phase of the signal at the output of the entire link was measured against input signal phase with additional phase detector. Tunnel conditions were simulated by changing second oven temperature. Observed was how the system compensates for the error induced by the long link temperature change.

First test was performed in laboratory conditions to get a rough knowledge about system performance. Then system was installed inside the climate chamber in order to stabilize system temperature and remove errors caused by ambient temperature changes. Following text of this chapter contains more detailed description of system tests.

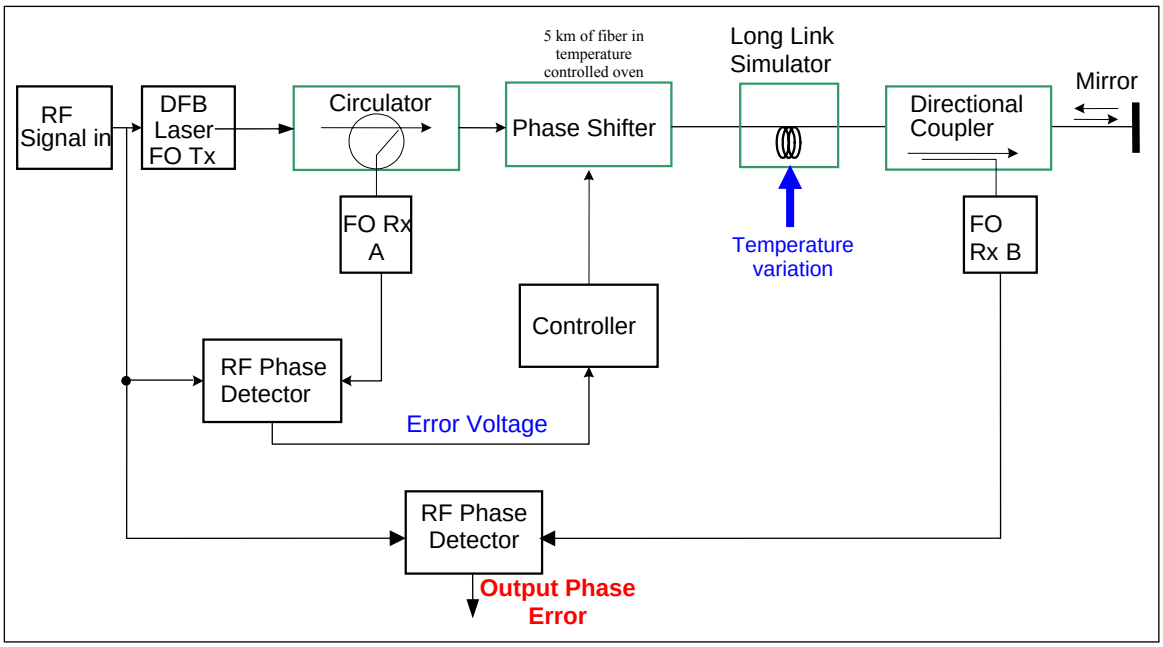

Figure 9.1.1: *FO link prototype test setup block diagram*

As mentioned above, first tests in were performed normal laboratory conditions where the software of Matlab GUI (section 7.3) and MSC1211 microcontroller (section 7.4) was debugged. Communication and data exchange between those controller elements was established. A photograph of very first, simplified system assembly is shown in figure 9.1.2. A phase lock in the system was successfully obtained but large output signal phase errors were observed. The reason for errors was large ambient temperature changes.

Figure 9.1.2: *Very first FO distribution system test.*

Next test was performed in the climate chamber. Great care has been taken to ensure the quality of cabling. Measurements of optical and RF power level were performed. Several amplifiers and attenuators were added to the setup to assure proper power levels at each point of the system. More detailed block diagram of the test system is shown in figure 9.1.3. This block diagram does not include power supply system.

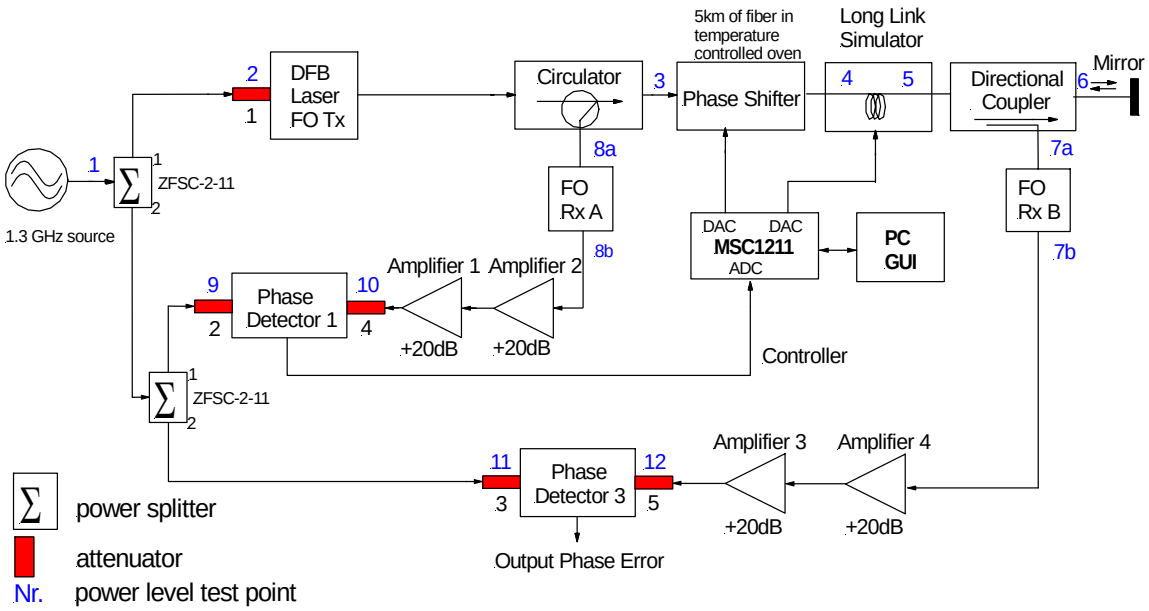

Figure 9.1.3: *Detailed block diagram of the FO system measurement setup.*

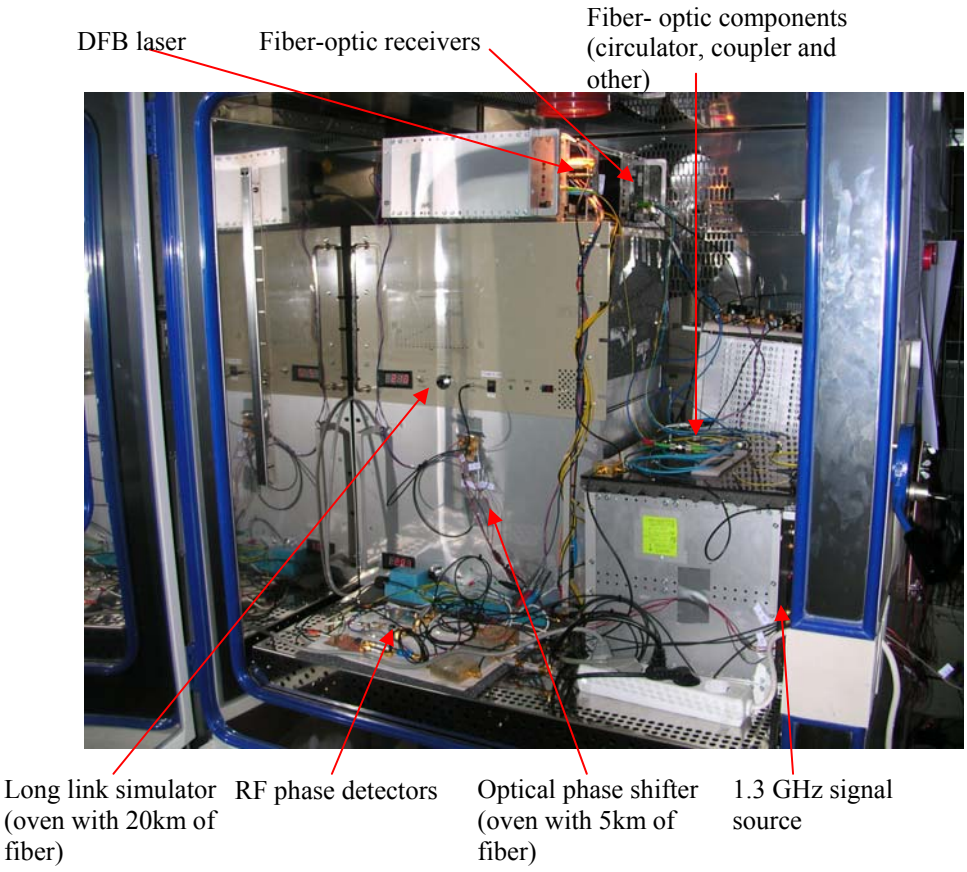

Figure 9.1.4: *FO distribution system inside of the climate chamber*

The assembly of the FO distribution system inside the climate chamber is shown in figure 9.1.4. During tests it was found that RF and fiber-optic cables hanging and laying loose in the system get influenced by mechanical vibration and air turbulences from the fans of the climate chamber and ovens. This was a source for significant level of measured noise.

Therefore all cables and FO components were fixed using soft foam which attenuated mechanical vibration. Foam plates can be seen under FO components and phase detectors in figure 9.1.4. This significantly reduced measured noise – a factor of three.

9.2. SYSTEM PERFORMANCE MEASUREMENTS

After system installation in the climate chamber the system step response was measured and calculation of the PID controller parameters was done (for details on this calculation see [10]). Then output signal phase error (short and long term) was measured. The phase error after providing temperature step on the long link with open controller loop was also measured for comparison with obtained closed loop results.

Unfortunately the long link simulator oven was comparably fast to the phase shifter oven. Because of significant phase shifter dead time it was difficult for the system to follow simulated phase error and a large output signal phase error was measured. Therefore the temperature step on the long link was decreased to about 1^{o}C. In the future it is planned to slow down the tunnel simulator. The response will then be much closer to normal accelerator environment conditions because expected are rather slow temperature changes there. The response of the phase shifter can be significantly sped up by removing the thermal insulation (cover) of the spool. Spool with fiber was purchased that is protected against the environment by a plastic cover (see figure 6.5.2), which is also a good thermal insulation and do not allow the air to flow directly on the fiber. The cover couldn't be removed because very delicate fiber is going through the holes in the cover and no tools to fixing again FC-APC type optical connectors were available in case of fiber damage. Improved spools have already been ordered with cover made of wire net.

Measured phase error on the output of the FO link with open feedback loop is shown in figure 9.2.1. Minimum and maximum phase values difference is ~260^{o}.

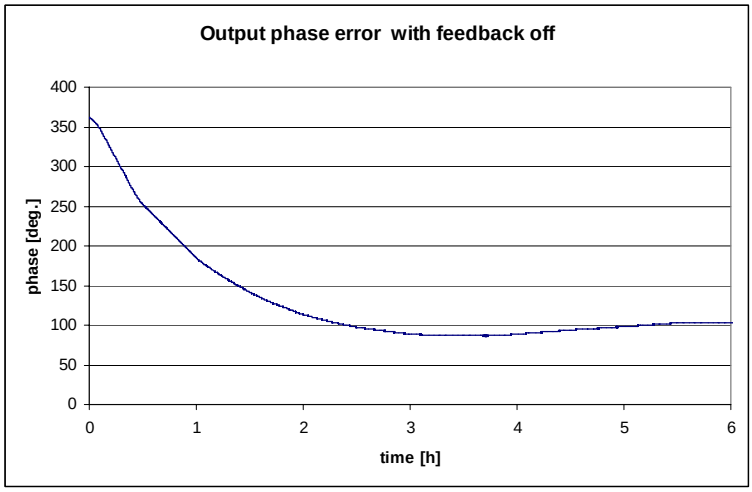

Figure 9.2.1: *Phase error with feedback switched off.*

Example of phase error after switching feedback on is shown in figure 9.2.2. The overshoot after applying the temperature step on the long link results from mentioned too fast long link simulator. After obtaining stable conditions output signal phase remained stable within approx. 2^{o} boundaries. Detected slow phase variations were caused by too small gain of the controller – small errors were causing very slow loop response and adjustments of the phase shifter were not precisely following phase changes in the long link simulator. It was difficult to set controller proportional gain higher than 20 – 30 because of significant phase

shifter dead time. Higher gain made system unstable. Fortunately there are ideas how to improve system performance – will be described in next section.

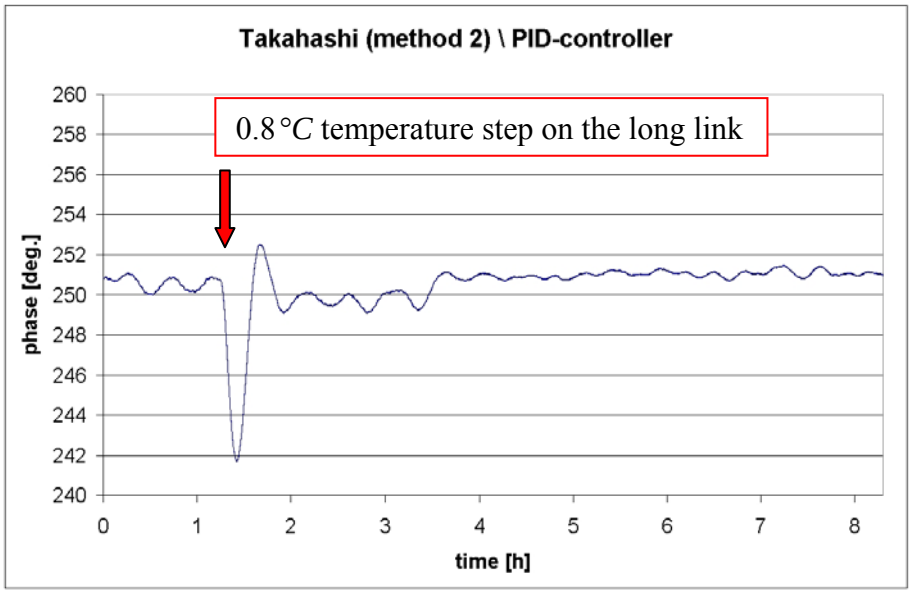

Figure 9.2.2: *Output phase error with closed feedback loop*

Measurement duration was little to short for reliable quantifying of the long term system stability but the result can be treated as reliable. The reason for short measurement was a problem with the PC and Matlab software. For unknown reason the GUI was hanging after randomly long period of time – between 5 and 15 hours. In the future careful investigation of this problem is planned and may be solved after getting newer version of Matlab software.

The measurement of the short term stability was also performed. The short term stability definition used here was that it is the maximum phase error (peak-to-peak) inside a window of time of given length. In this case 1 minute long time window was used. There is a function implemented in the GUI that automatically (in every sampling time period) finds maximum phase difference during last 60 seconds. It can be described it as a “sliding” window.

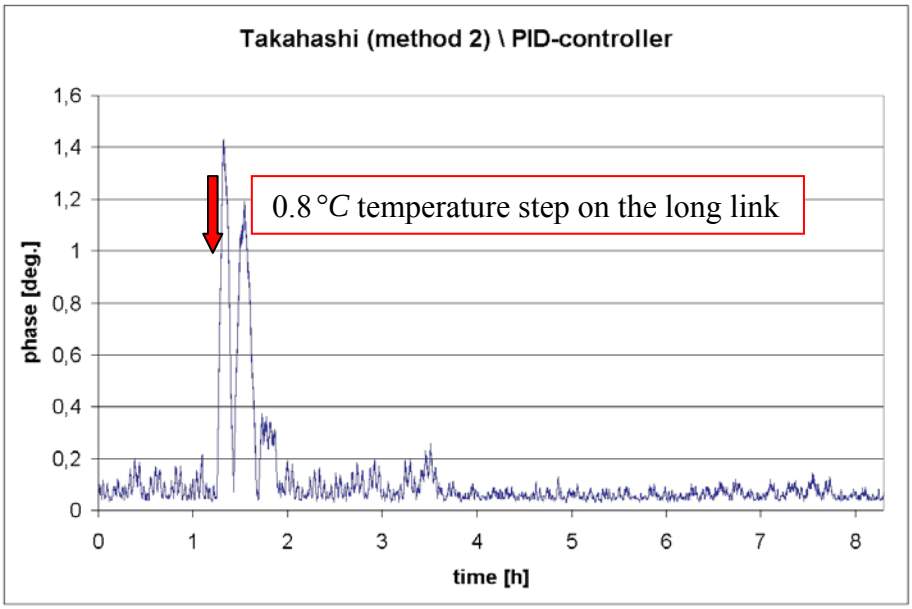

Figure 9.2.3: *Short term stability measurement results*

The result of short term stability measurement is shown in figure 9.2.3. Again, the overshoot after temperature step on the long link was caused by to fast long link simulator. After the overshoot the short term error does not exceed 0.3 ps. It is significantly better than the requirement of 1 ps.

10. SUMMARY, CONCLUSIONS AND FUTURE PLANS

The design of an analogue fiber-optic link with feedback loop suppressing phase errors to the level pf 1 ps on link distances up to 20 km is described in this report. Requirements on the system and system concept are described. Detailed error considerations are performed. Design issues and performance measurements of system components are described. Complex electronic hardware like laser transmitter and temperature controlled oven has been developed. System controller software with graphic user interface has been developed to enable optimization of system controller parameters for best stability performance. System installation in the climate chamber and performance measurements were performed and promising results obtained - long term stability of 2 ps (required 5 ps) and short term stability of 0.3 ps (required 1 ps) was obtained. Results were obtained for limited long link temperature variations but experience gained during tests will allow further improvements of the system performance.

FUTURE PLANS

There are many plans to improve system performance. First phase shifter response will be will be faster after using better fiber spool with no thermal insulation (more details in section 9.2). There is also a plan to put a fan blowing air over a wire heater inside the oven. This will react much faster than the large, high power TEC element of the oven.

Another way of phase shifter improvement is the use of motorized Optical Delay Line (ODL). A step motor driven bidirectional device with phase range of 330 ps and 40 fs resolution was found. The range is not sufficient to compensate for phase errors in links longer than 500m but it is sufficient for TTF2 operation. The ODL can also be used in series with the fiber spool in the oven to improve system response. Experiments with the ODL are planned.

More plans concerning the system are listed below:

- Improvement of the oven thermal insulation – especially the oven 1 has only one layer of thermal insulation installed. Significant ambient temperature sensitivity is observed.
- Improvement of controller software. First of all, the GUI hanging after several hours must be fixed. There also several GUI improvements would be useful like better data storage functions and more flexible user interface.
- A 19” type crate for the system electronics will be prepared. Card type system components (phase detectors, amplifiers and so on) will be built. Good, simplified and shorted cable layout may significantly improve system performance. A crate will also be a step towards future system installation in the accelerator environment.
- Conversion of PID controller equations form matlab to C language code and preparation of stand-alone system controller with the MSC1211 is planned. Proper software must be prepared for this purpose.
- As mentioned in section 7.4 a PCB for the MSC1211 microcontroller will be designed to avoid using evaluation PCB. It will be a PCB suited for the system 19” crate.

- More investigations on system components sensitivity to temperature will be performed. Particularly the phase detectors should be replaced with better, less sensitive to temperature and with better linearity devices. A newer phase detector chip – HMC439 is supposed to be better for this application.

11. ACKNOWLEDGEMENT

We acknowledge the support of the European Community Research Infrastructure Activity under the FP6 "Structuring the European Research Area" program (CARE, contract number RII3-CT-2003-506395)

12. REFERENCES

[1] http://tesla.desy.de [TESLA Home Page];
[2] http://xfel.desy.de [XFEL Home Page];
[3] K. Czuba, H. C. Weddig, “Design considerations for the RF phase reference distribution system for X-Ray FEL and TESLA”, Proc. SPIE, Vol. 5484, pp 148-152, (2004);
[4] J. Frish, D. G. Brown, E. L. Cisneros, “The RF Phase Distribution and Timing System for the NLC”, pp 745-747, XX International Linac Conference, Monterey, California, 2000;
[4] W. S. Levine, The Control Handbook, pp 198-207, CRC Press Inc. 1996.
[5] Abdul Aziz Ishak: Dept. of Chemical Engineering, University Technology MARA, MALAYSIA http://aabi.tripod.com/optimumpid/cohen/optimum-pid-cohencoon.htm
[6] Heinz Unbehauen: Regelungstechnik (2) 8. Edition Vieweg
[7] A.Angermann: Matlab-Simulink-Stateflow 2.Edition Oldenburg p.233
[8] H.-J.Bartsch: Taschenbuch mathematischer Formeln 17.Edition Fachbuchverlag Leipzig p. 440.
[9] Lothar Papula: Mathematik fuer Ingenieure 1 6. Edition Vieweg p. 358
[10] Frank Eints, „Development of an Algorithm for a RF Fiber-optic Phase Controller”, B.Sc Thesis, Hamburg 2004

13. APPENDIX 1

The following pictures contain detailed schematic diagrams of oven 1 described in section 6.1

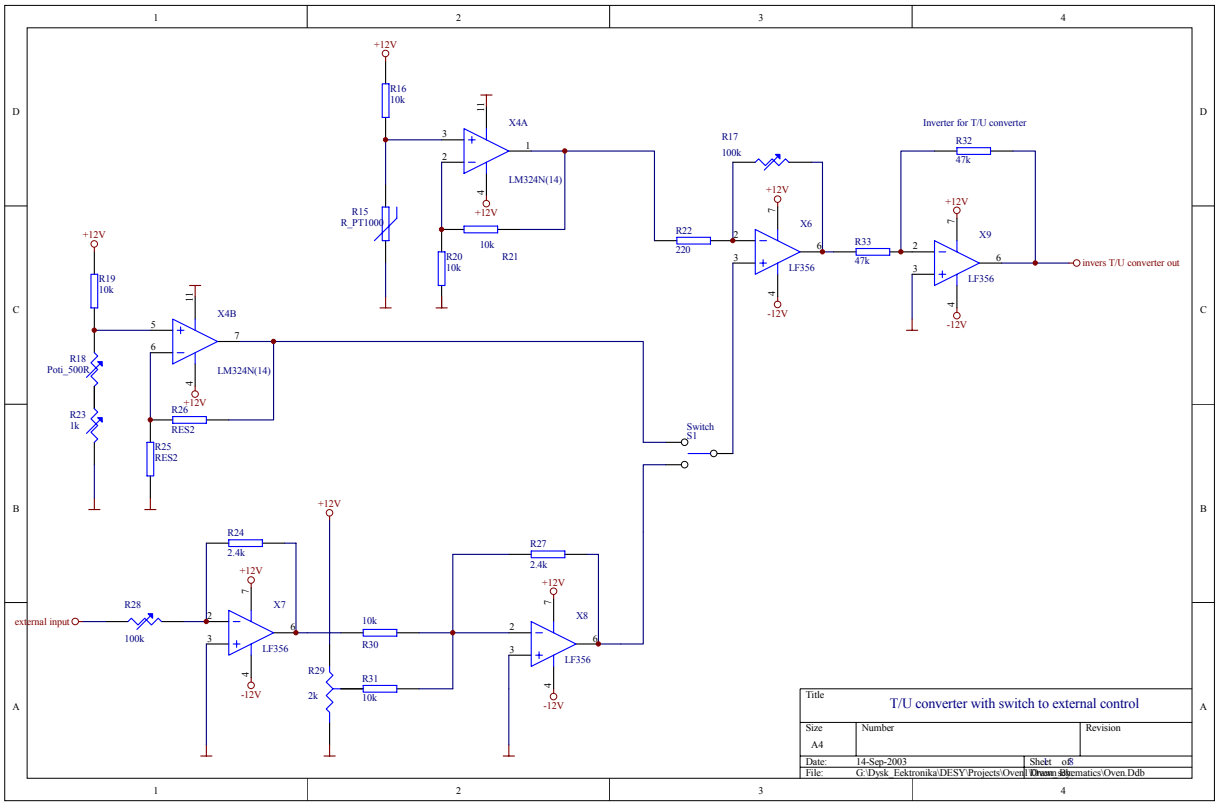

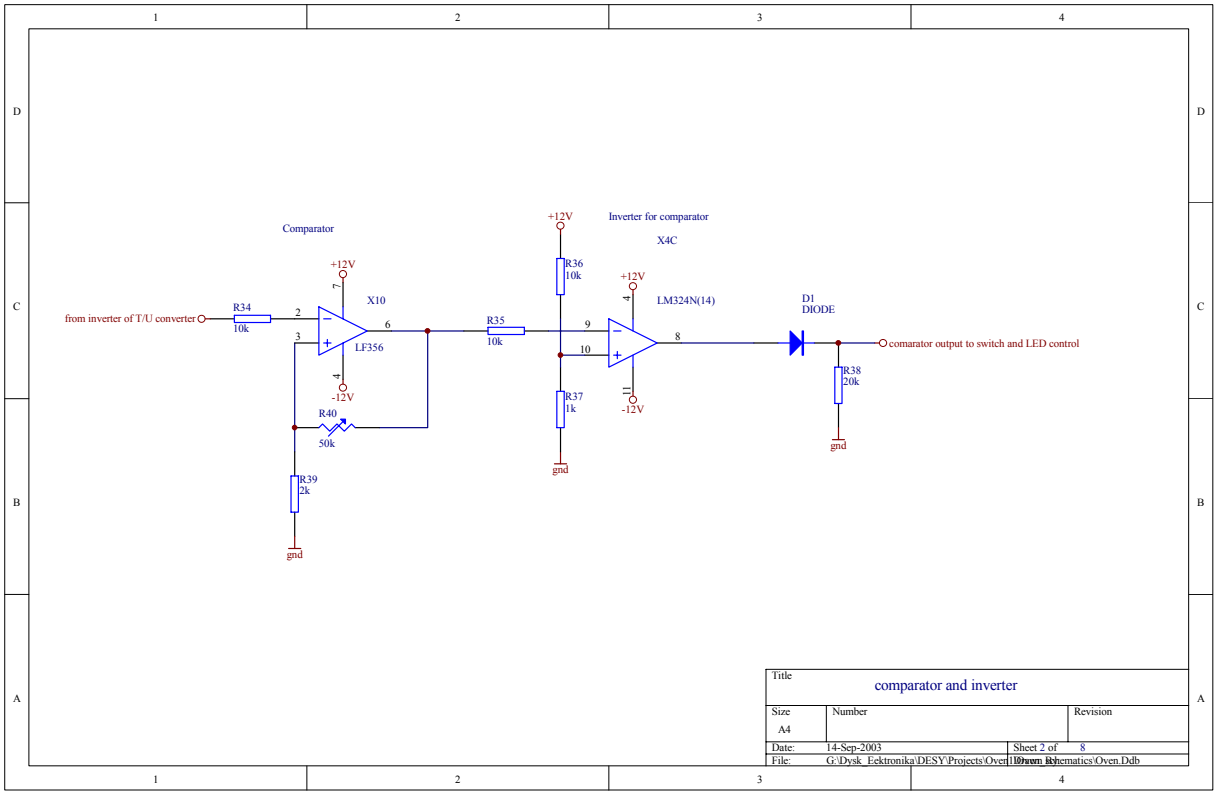

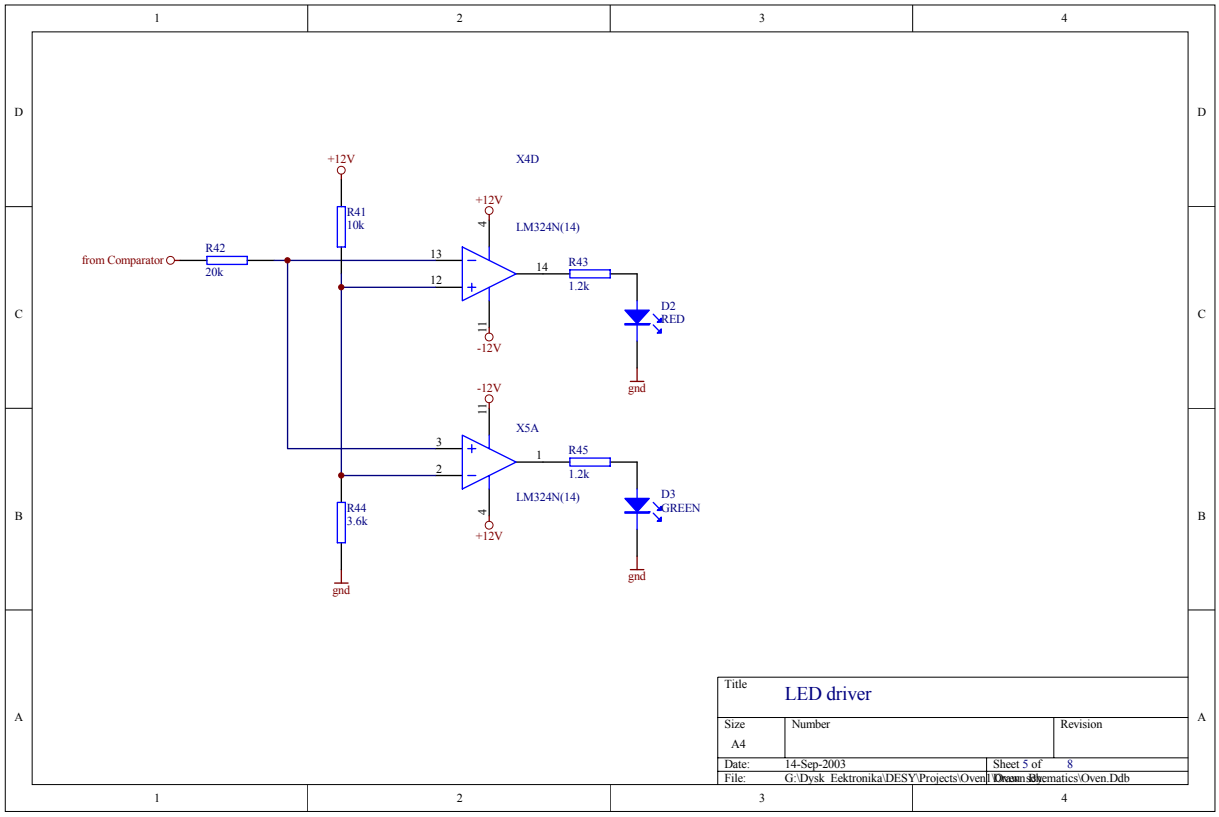
+12V
X4D
R41
10k
+12V
LM324N(14)
from Comparator
R42
20k
13
12
14
R43
1.2k
D2
RED
-12V
gnd
-12V
X5A
3
2
1
R45
1.2k
LM324N(14)
D3
GREEN
R44
3.6k
+12V
gnd
gnd
Title
LED driver
Size
A4
Number
Revision
Date:
14-Sep-2003
Sheet 5 of 8
File:
G:\Dysk Eektronika\DESY\Projects\Oven\Drawn Schematics\Oven.Ddb

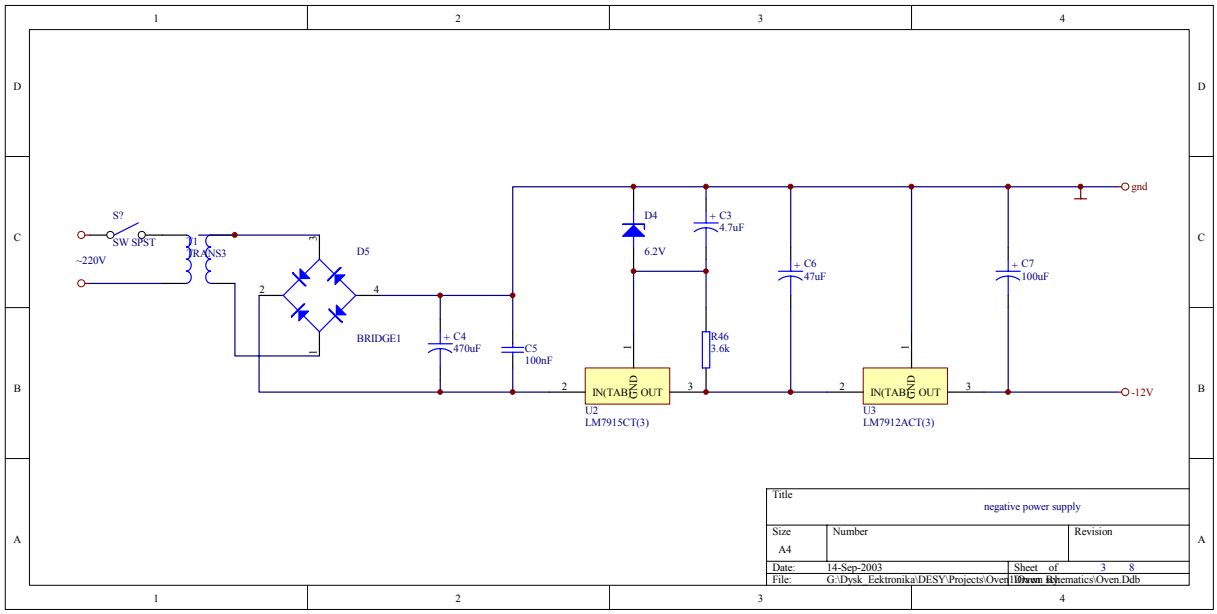
S?
SW SPST
~220V
T1
TRANS3
D5
BRIDGE1
D4
6.2V
+ C3
4.7uF
+ C6
47uF
+ C7
100uF
gnd
+ C4
470uF
C5
100nF
R46
3.6k
IN(TAB)
GND
OUT
U2
LM7915CT(3)
U3
LM7912ACT(3)
-12V
Title
negative power supply
Size
A4
Number
Revision
Date:
14-Sep-2003
Sheet 3 of 8
File:
G:\Dysk Eektronika\DESY\Projects\Oven\Drawn Schematics\Oven.Ddb

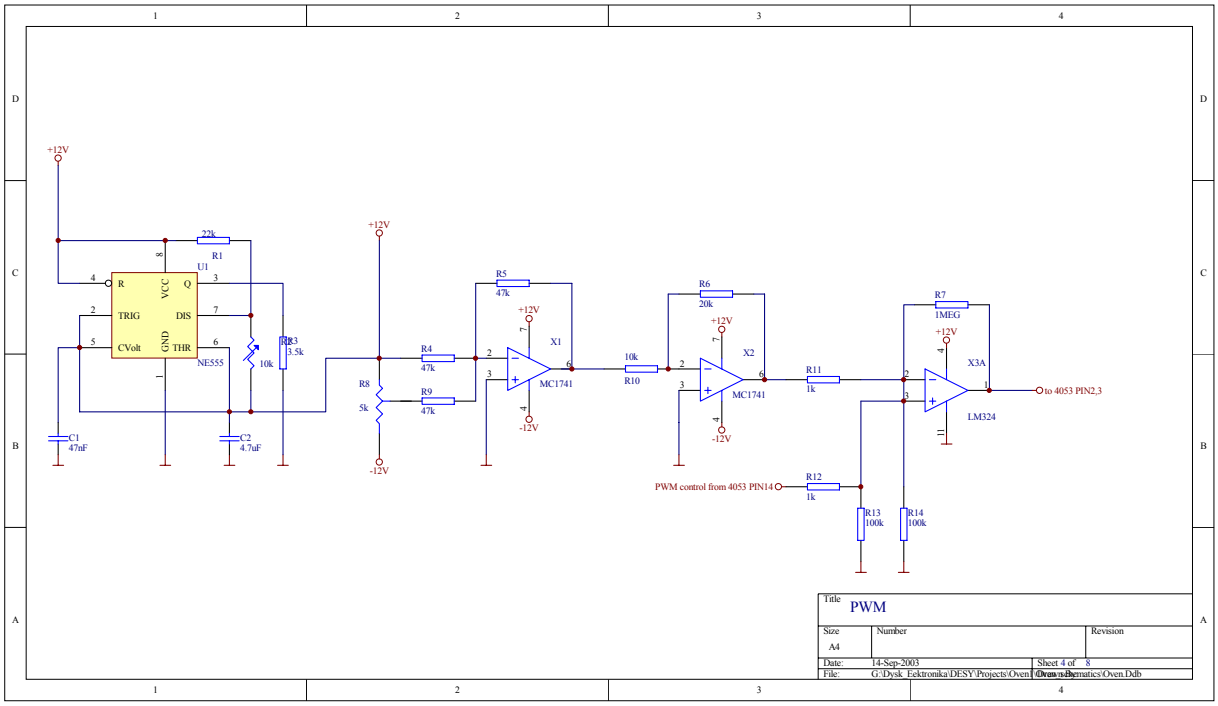
+12V
22k
R1
U1
NE555
R
VCC
Q
TRIG
DIS
CVolt
GND
THR
10k
R3
3.5k
C1
47nF
C2
4.7uF
R8
5k
R4
47k
R9
47k
R5
47k
X1
MC1741
-12V
10k
R10
R6
20k
X2
MC1741
R11
1k
R7
1MEG
X3A
LM324
to 4053 PIN2,3
PWM control from 4053 PIN14
R12
1k
R13
100k
R14
100k
Title
PWM
Size
A4
Number
Revision
Date:
14-Sep-2003
Sheet 4 of 8
File:
G:\Dysk Eektronika\DESY\Projects\Oven\Oven Schematics\Oven.Ddb

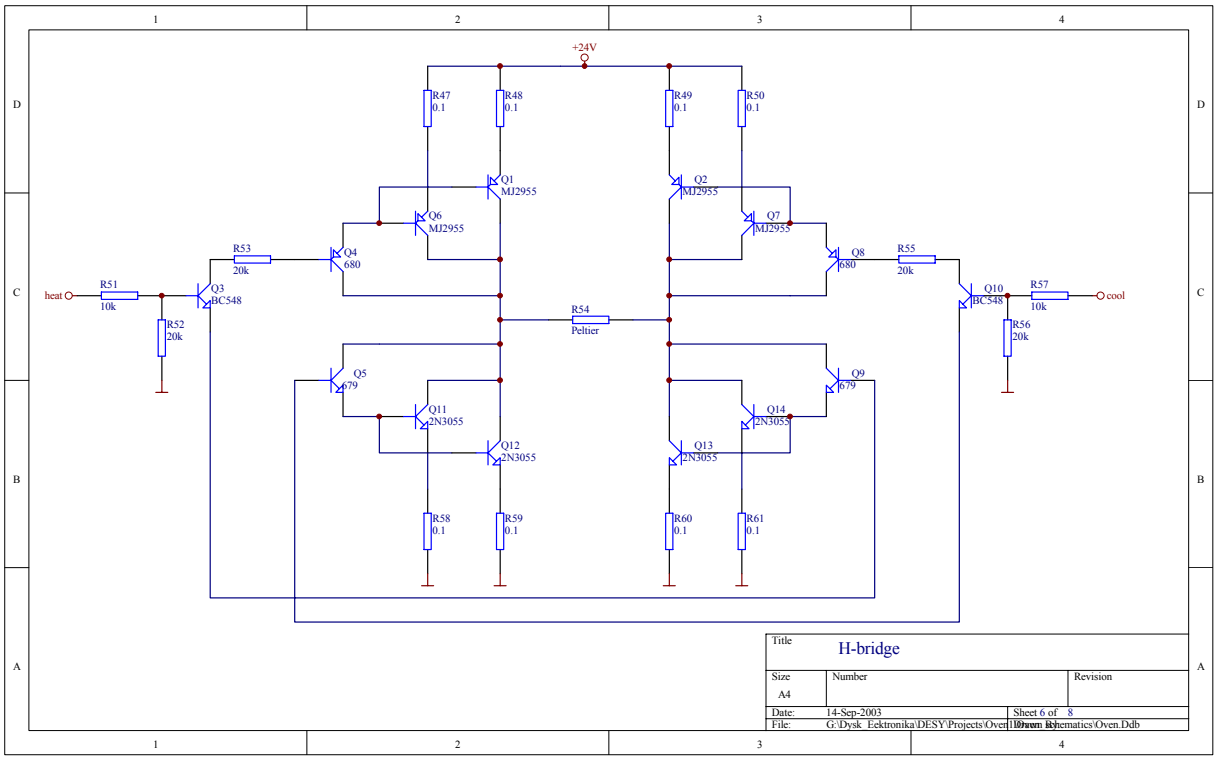
+24V
R47
0.1
R48
0.1
R49
0.1
R50
0.1
Q1
MJ2955
Q2
MJ2955
Q6
MJ2955
Q7
MJ2955
R53
20k
Q4
680
Q8
680
R55
20k
heat
R51
10k
Q3
BC548
R52
20k
R54
Peltier
Q10
BC548
R57
10k
cool
R56
20k
Q5
679
Q9
679
Q11
2N3055
Q14
2N3055
Q12
2N3055
Q13
2N3055
R58
0.1
R59
0.1
R60
0.1
R61
0.1
Title
H-bridge
Size
A4
Number
Revision
Date:
14-Sep-2003
Sheet 6 of 8
File:
G:\Dysk Eektronika\DESY\Projects\Oven\Oven Schematics\Oven.Ddb

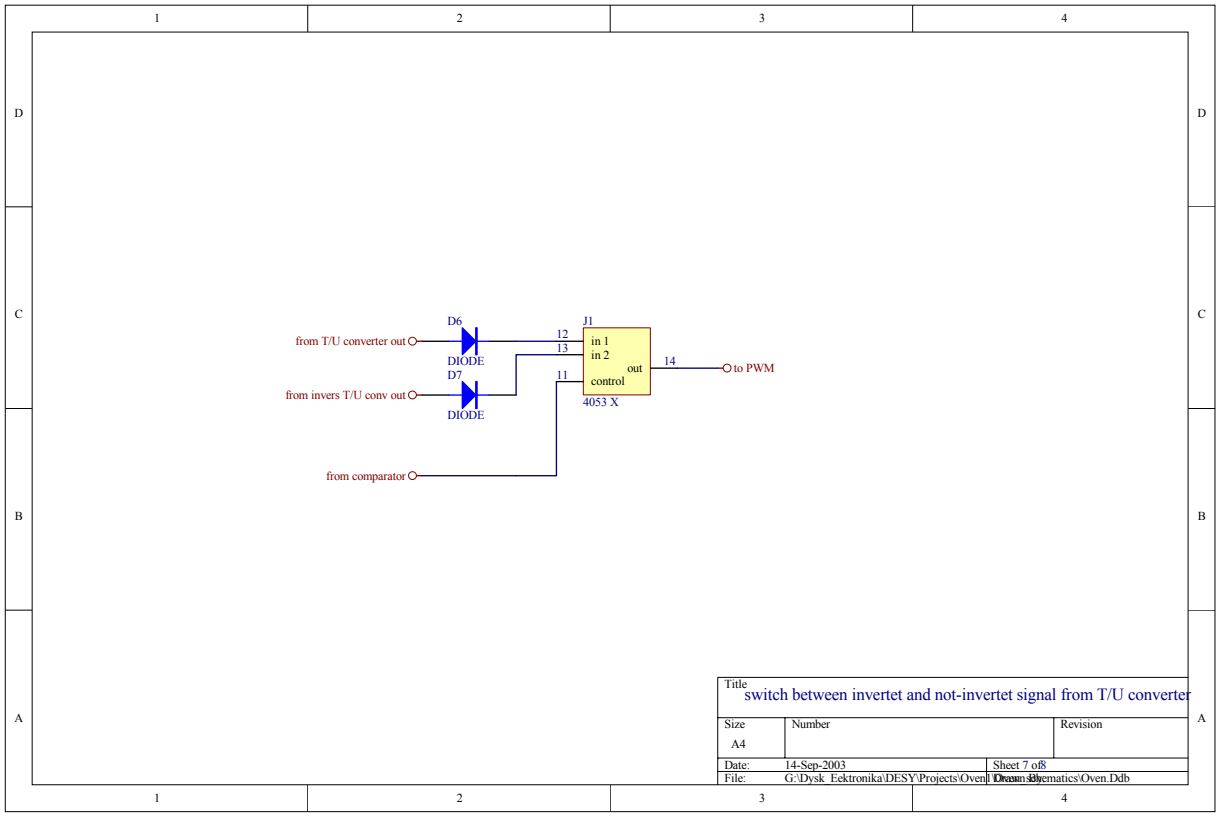
from T/U converter out
D6
DIODE
12
13
J1
in 1
in 2
out
control
4053 X
14
to PWM
from invers T/U conv out
D7
DIODE
11
from comparator
Title
switch between invertet and not-invertet signal from T/U converter
Size
A4
Number
Revision
Date: 14-Sep-2003
Sheet 7 of 8
File: G:\Dysk_Eektronika\DESY\Projects\Oven\Oven Schematics\Oven.Ddb

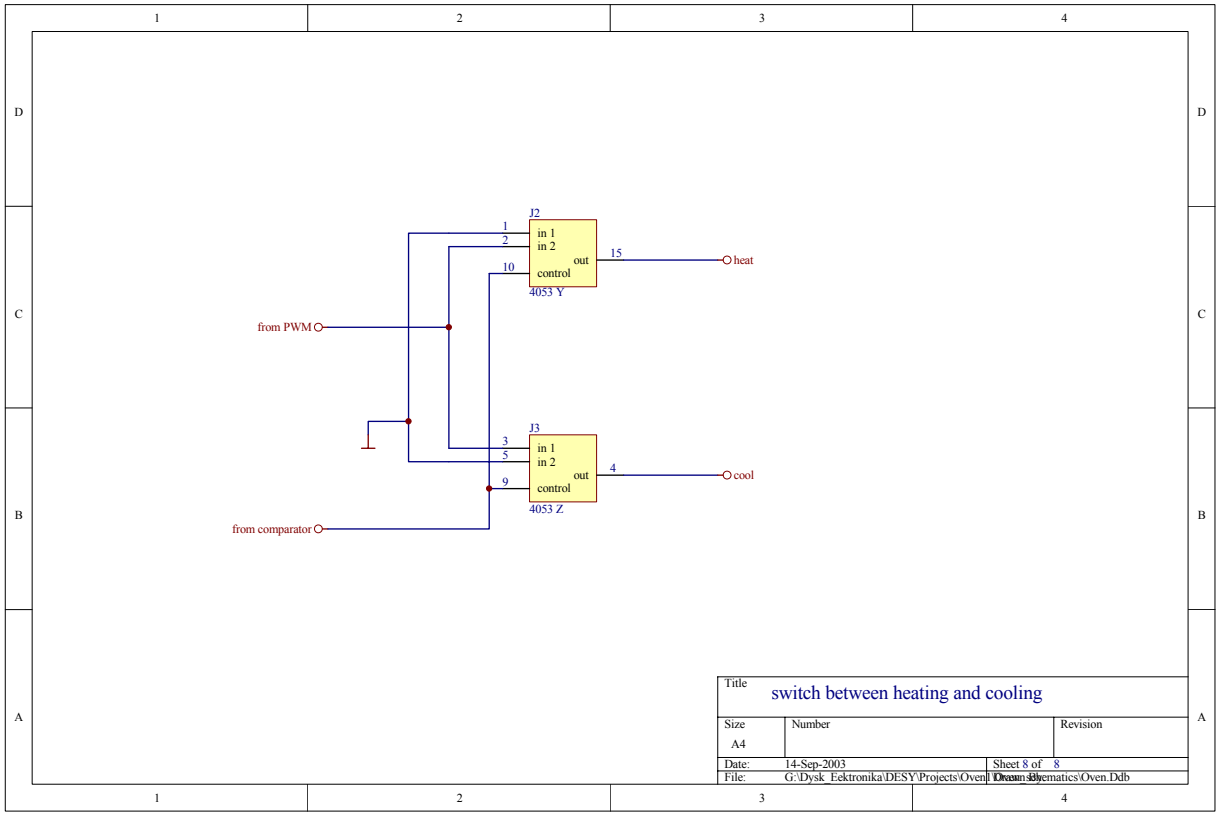
J2
1
2
in 1
in 2
out
control
10
4053 Y
15
heat
from PWM
J3
3
5
in 1
in 2
out
control
9
4053 Z
4
cool
from comparator
Title
switch between heating and cooling
Size
A4
Number
Revision
Date: 14-Sep-2003
Sheet 8 of 8
File: G:\Dysk_Eektronika\DESY\Projects\Oven\Oven Schematics\Oven.Ddb